Mineral Dust in the Atmosphere

Stavros Solomos
National Observatory of Athens

May 2019

Layout

- Natural Aerosols
- Atmospheric Aerosol Feedbacks
- Model - Satellite Synergies
- Dust properties
- Dust emissions
- Haboobs
- Effects on clouds
- Ongoing & Future Work
- NOA Antikythera Climate Change Observatory

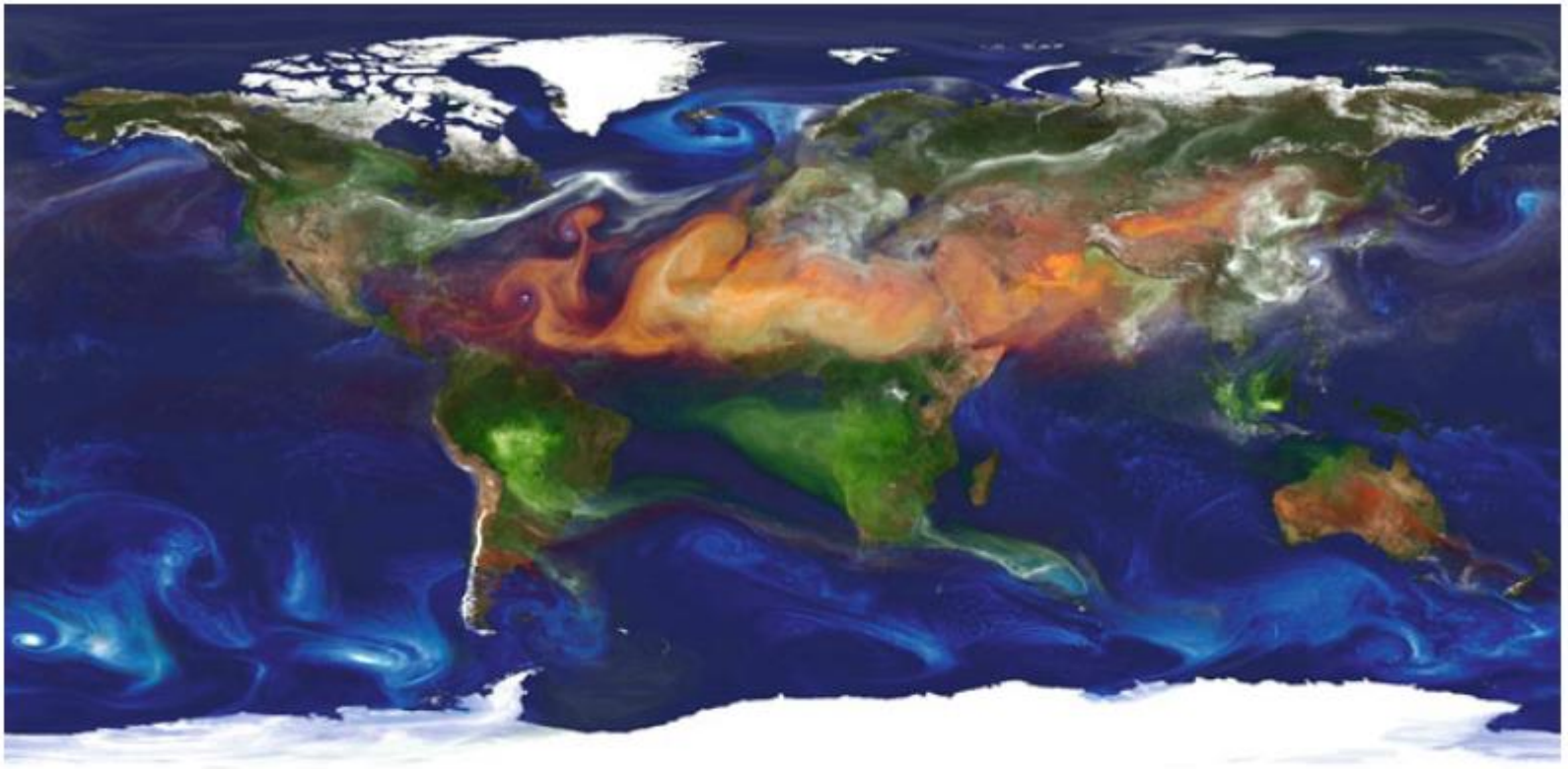

Fig. 1.1 NASA's GEOS-5 simulation, showing the four main aerosols: mineral dust from deserts (*red*), sea salt from spray (*blue*), soot and smoke from fires (*green*) and sulphate particles from fossil fuel combustion and volcanoes (*white*). Source: http://geos5.org

Aerosols from Natural Sources

Dust

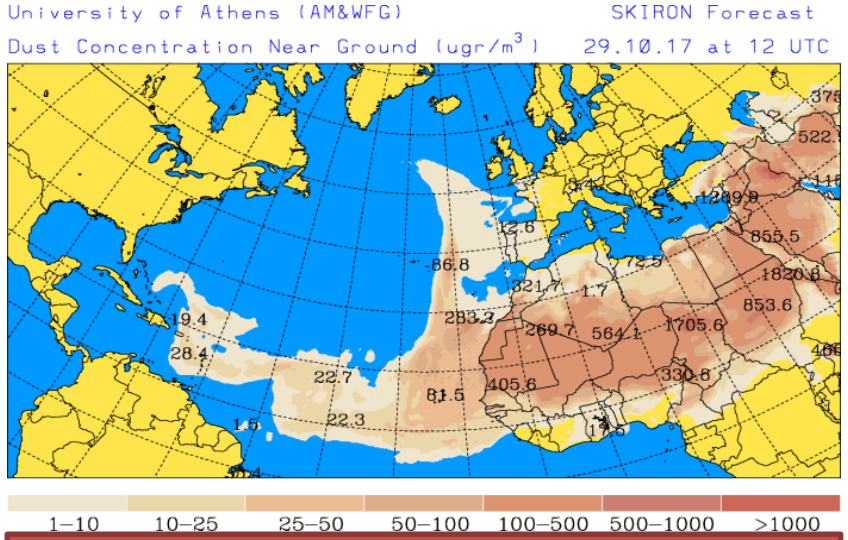

Biomass burning

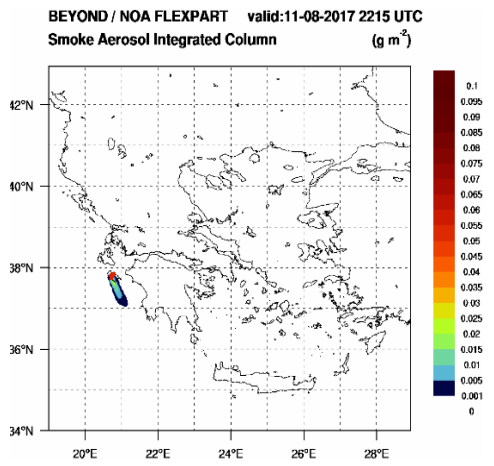

Volcanic ash

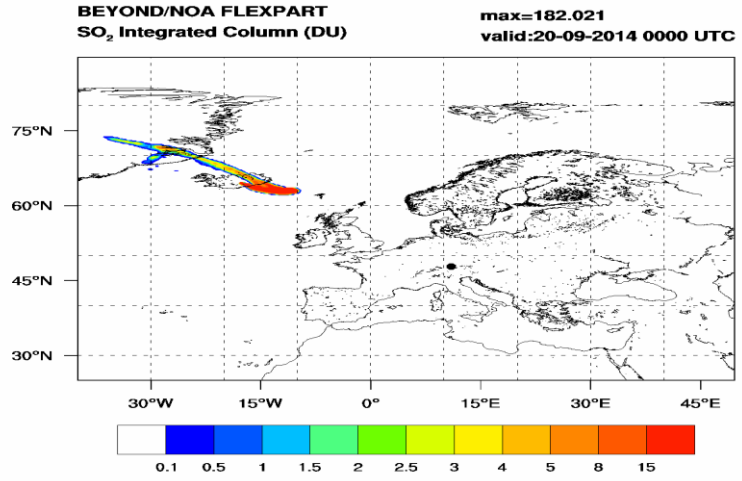

Sea salt

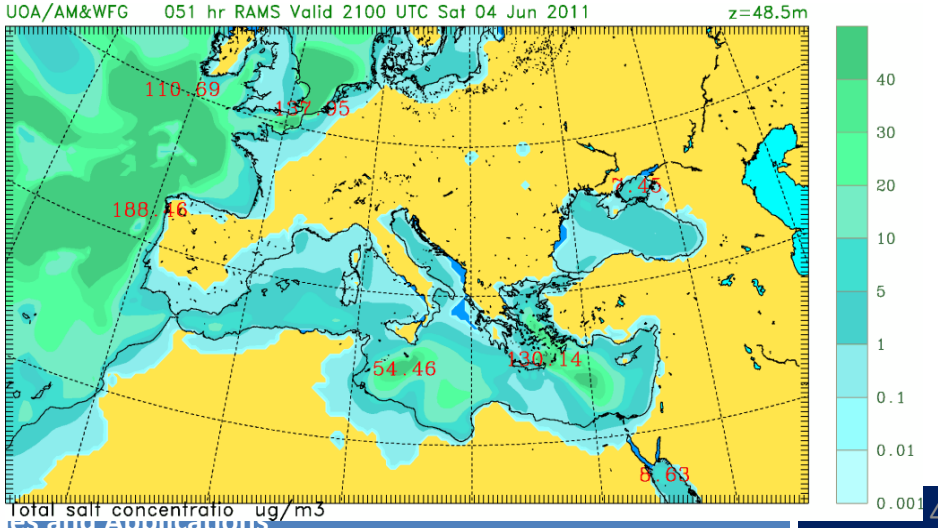

Desert Dust Emissions

Local Sand/dust storms (haboobs)

Long Range Transport

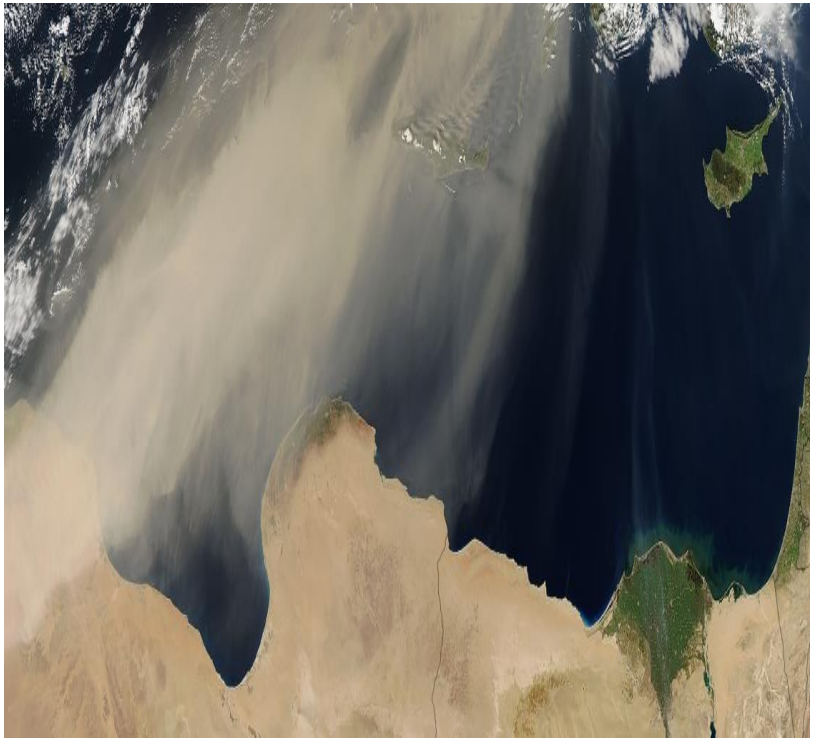

Dust Mineralogy

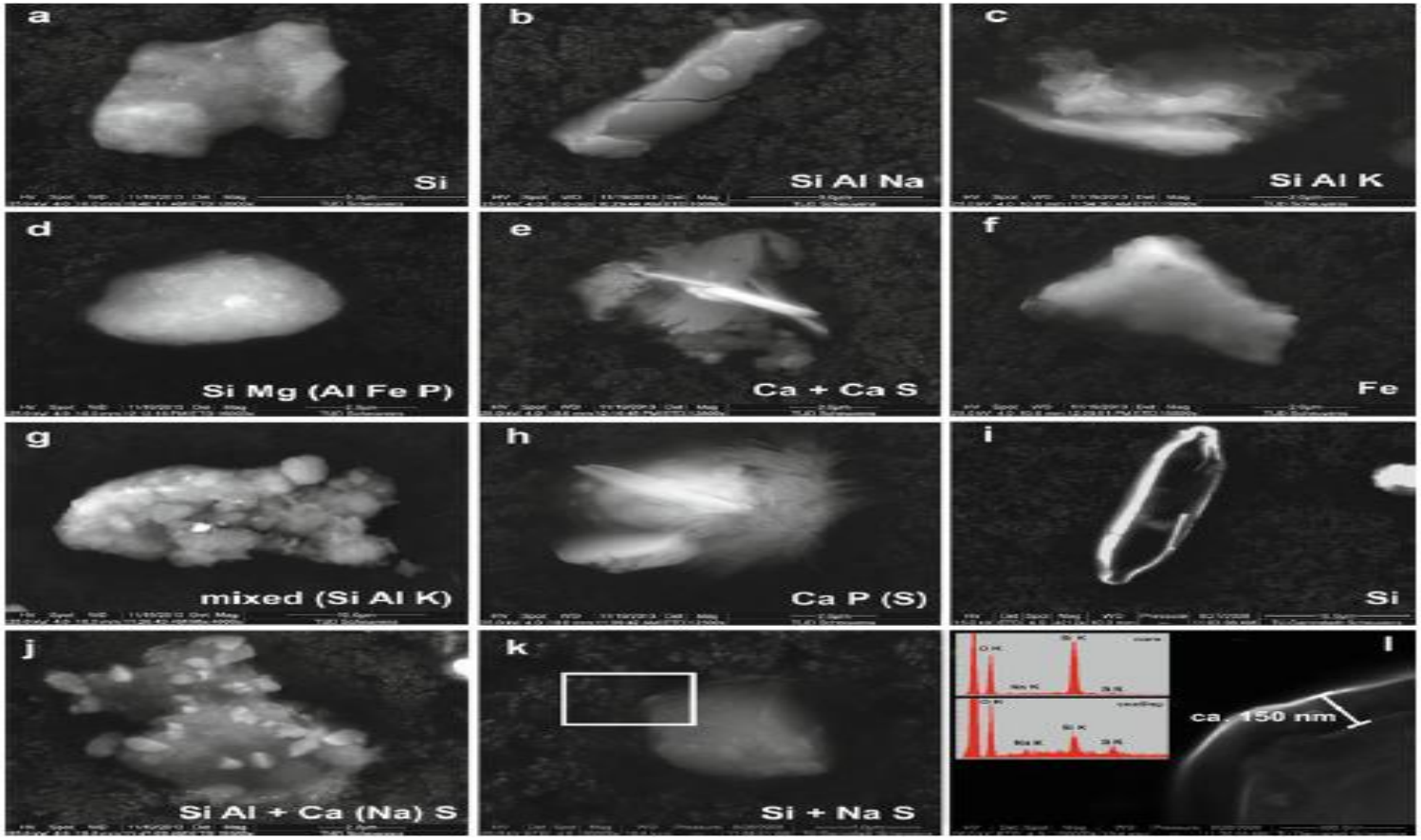

Fig. 2.1 Secondary electron images of typical dust particles of northern Africa collected during the SAMUM I campaign in Morocco. At the bottom of the images, the major elements analyzed by energy-dispersive X-ray technique (EDX) are labelled. In the following, common atmospheric minerals with the specified composition (and matching the morphology of the particle) are given in parenthesis. (**a**) Si-rich particle (quartz), (**b**) Na-bearing aluminosilicate (albite), (**c**) K-bearing aluminosilicate (illite), (**d**) Mg-dominated silicate (palygorskite), (**e**) Ca sulfate and Ca-dominated mineral (gypsum on calcite), (**f**) Fe-dominated mineral (iron oxide or iron hydroxide), (**g**) complex internally mixed aluminosilicate with individual Fe-dominated phase (bright spot in center), (**h**) Ca-P-S-bearing particle (biological?), (**i**) Si-dominated particle (opaline diatom), (**j**) aluminosilicate (kaolin group?) with Ca(Na) sulfate (gypsum, thenardite, glauberite?), and (**k**) Si-rich particle (quartz) with sulfate coating (overview). (**l**) Detail of coating with EDX spectra for rim and core of the particle

Dust Size Distributions

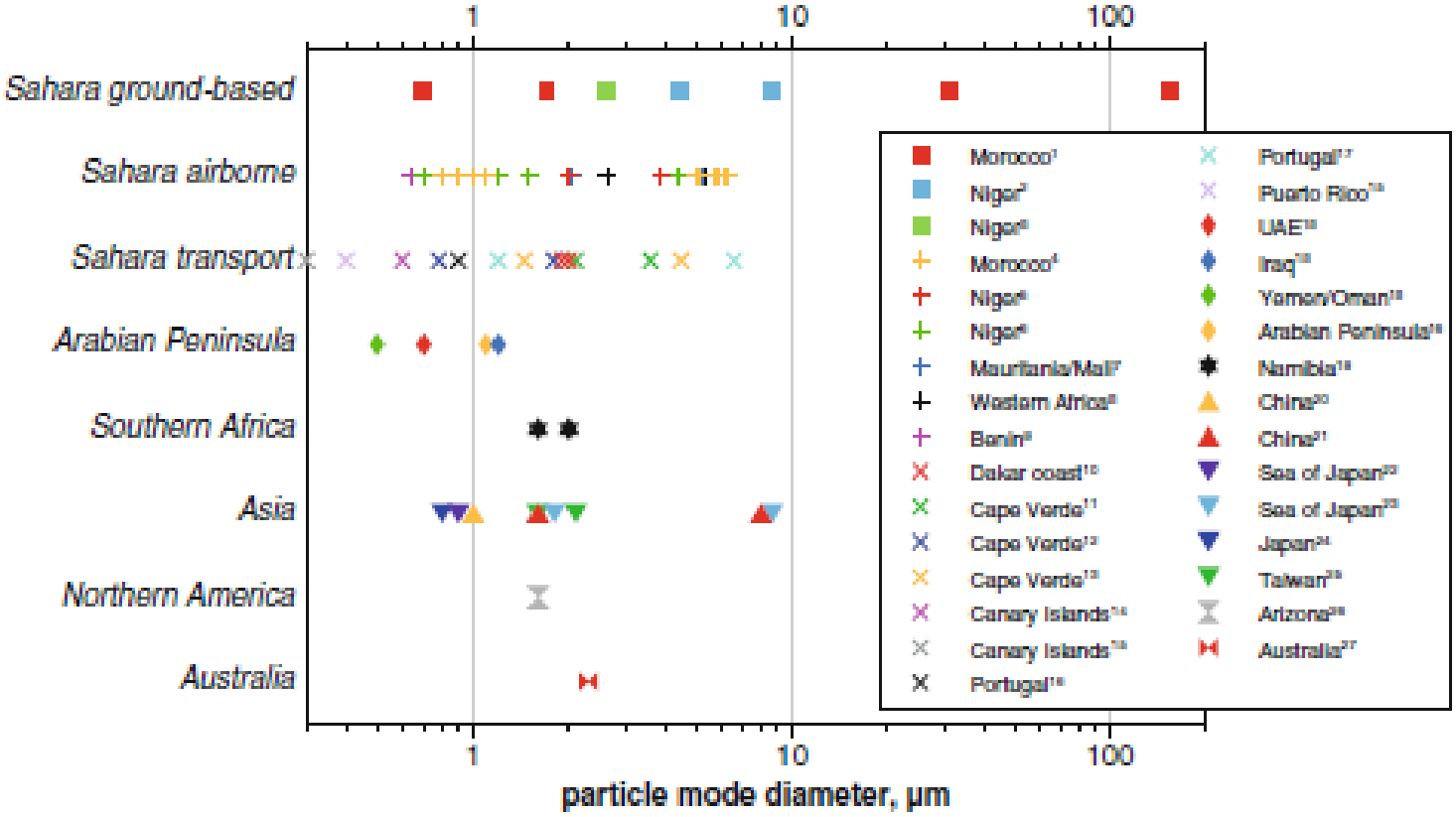

Fig. 2.2 Number modal diameters detected by atmospheric measurements for different dust situations. *1* Kandler et al. (2009), *2* Rajot et al. (2008), *3* Sow et al. (2009), *4* Weinzierl et al. (2009), *5* Osborne et al. (2008), *6* Chou et al. (2008), *7* Ryder et al. (2013), *8* Johnson and Osborne (2011), *9* Crumeyrolle et al. (2011), *10* McConnell et al. (2008), *11* Haywood et al. (2003a), *12* Schladitz et al. (2011), *13* Weinzierl et al. (2011), *14* de Reus et al. (2000), *15* Maring et al. (2003), *16* Bates et al. (2002), *17* Wagner et al. (2009), *18* Reid et al. (2008), *19* Haywood et al. (2003b), *20* Kim et al. (2004), *21* Zhou et al. (2012), *22* Quinn et al. (2004), *23* Clarke et al. (2004), *24* Kobayashi et al. (2007), *25* Chang et al. (2010), *26* Peters (2006), *27* Shao et al. (2011)

Mineral Dust Sources

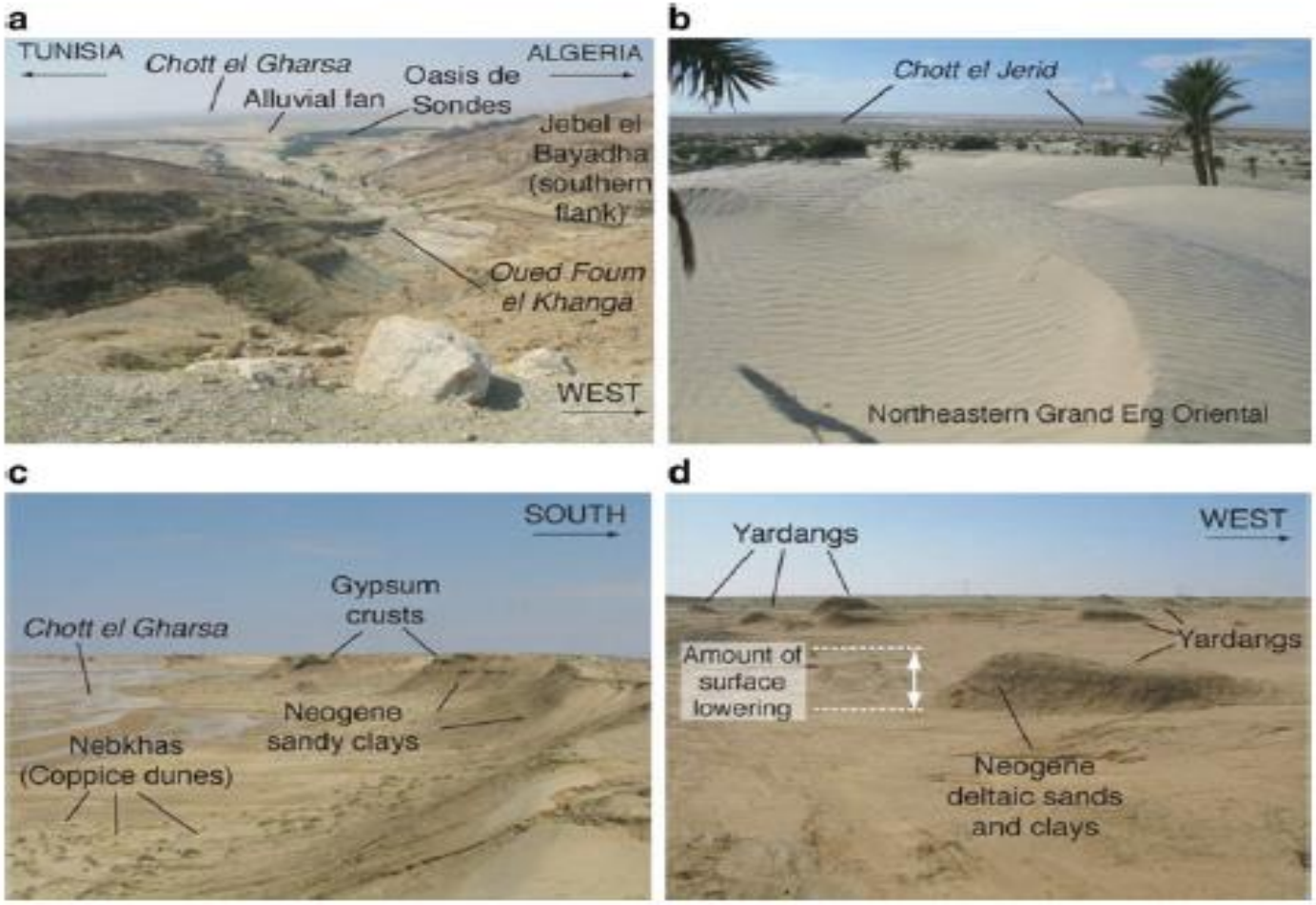

Fig. 3.1 Geomorphic settings in the Sahara Desert that are common dust sources: (**a**) wadi and alluvial fan of the Oued Foum el Khanga, draining the Atlas Mountains of Tunisia and Algeria; (**b**) dunes of northernmost part of Grand Erg Oriental adjacent to southeastern side of Chott (playa) el Jerid, Tunisia; (**c**) fine-grained sediments in Chott el Gharsa, derived from sandy clays of Neogene age, northeast of Tozeur, Tunisia; (**d**) yardangs eroded into Neogene deltaic sands and clays, southern Tunisia (Photographs by D.R. Muhs)

Mineral Dust Sources

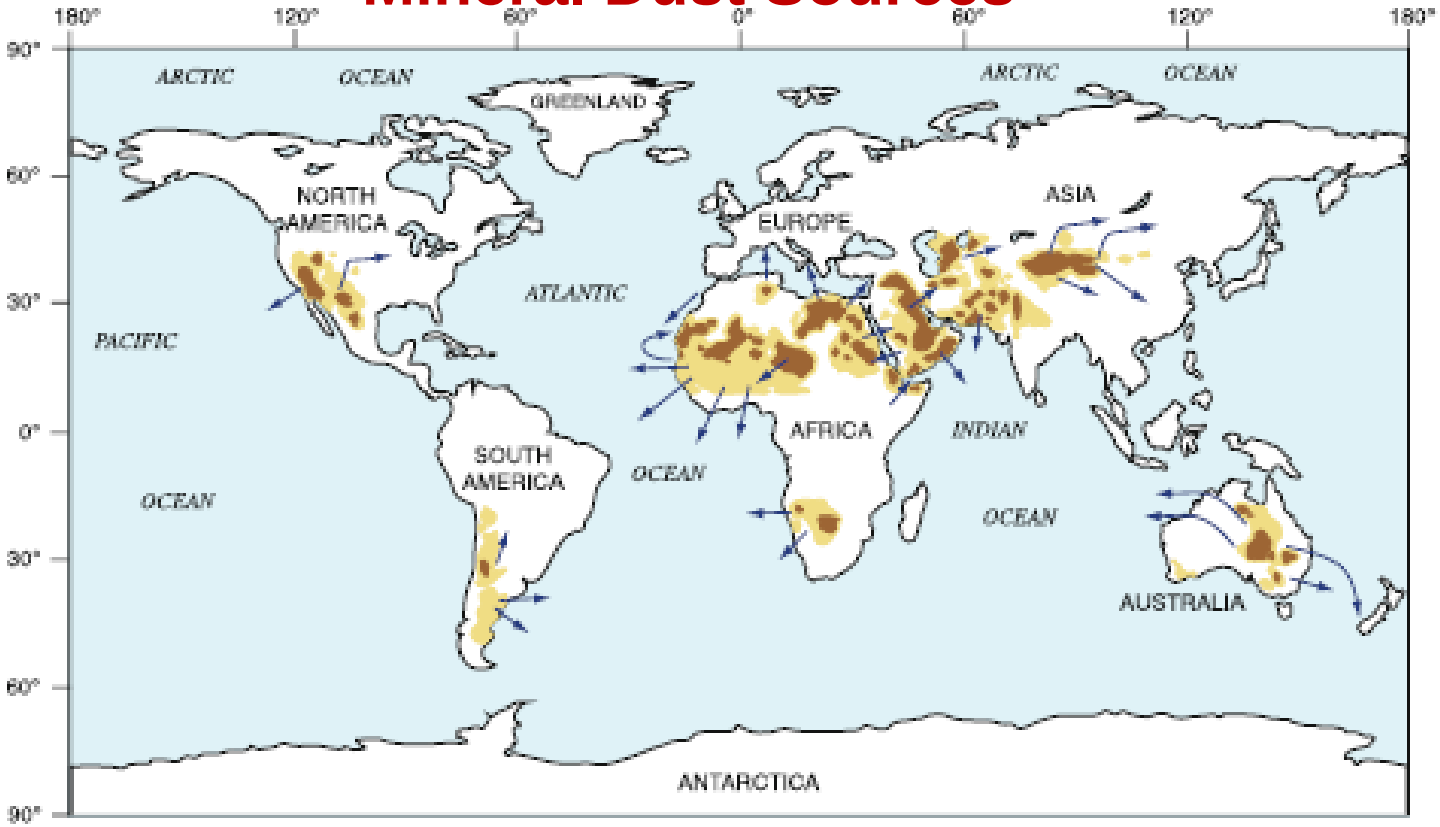

Fig. 3.2 Map of global dust sources, based on multiple years of satellite imagery, derived from frequency of occurrence (number of days) where the TOMS absorbing aerosol index (*AAI*) is greater than 0.7 (significant amounts of dust or smoke) or 1.0 (abundant dust or smoke). For comparison, nonabsorbing aerosols such as sulfate and sea salt yield negative AAI values; clouds yield values near zero; ultraviolet-absorbing aerosols such as dust and smoke yield positive values (Prospero et al. 2002). *Dark brown* is 21–31 days; *yellow* is 7–21 days (Redrawn from Fig. 4 of Prospero et al. 2002). *Blue arrows* indicate typical dust transport pathways, based on interpretation of MODIS imagery from Terra and Aqua satellites by the authors

Mineral Dust Aging

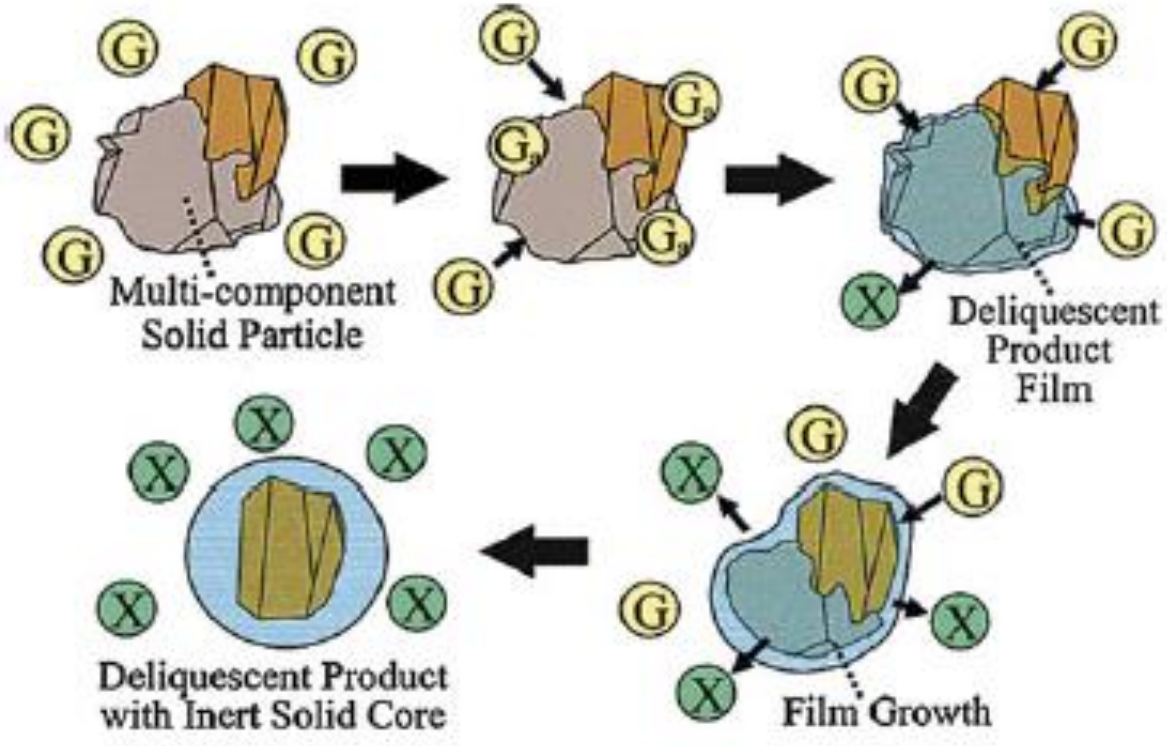

Fig. 4.1 Pictorial representation of changes in a composite mineral dust particle as it is processed in the atmosphere (Reprinted with permission from Usher et al. (2003). Copyright (2003) American Chemical Society)

Dust Emission Mechanisms

Fig. 5.2 Mechanisms for dust emission. (**a**) Dust emission by aerodynamic lift, (**b**) by saltation bombardment and (**c**) through disaggregation (Adapted from Shao et al. 2011)

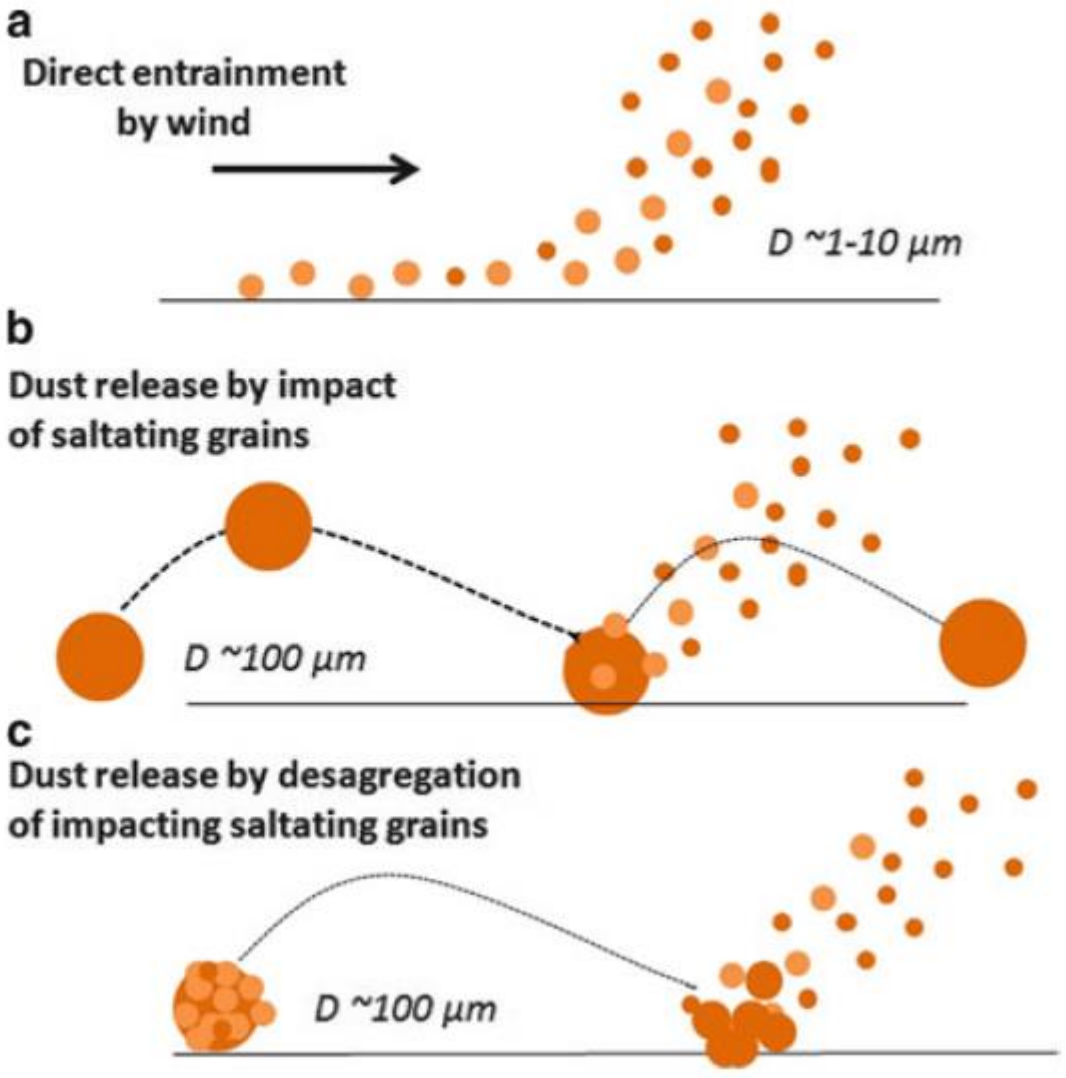

Synoptic scale dust transport

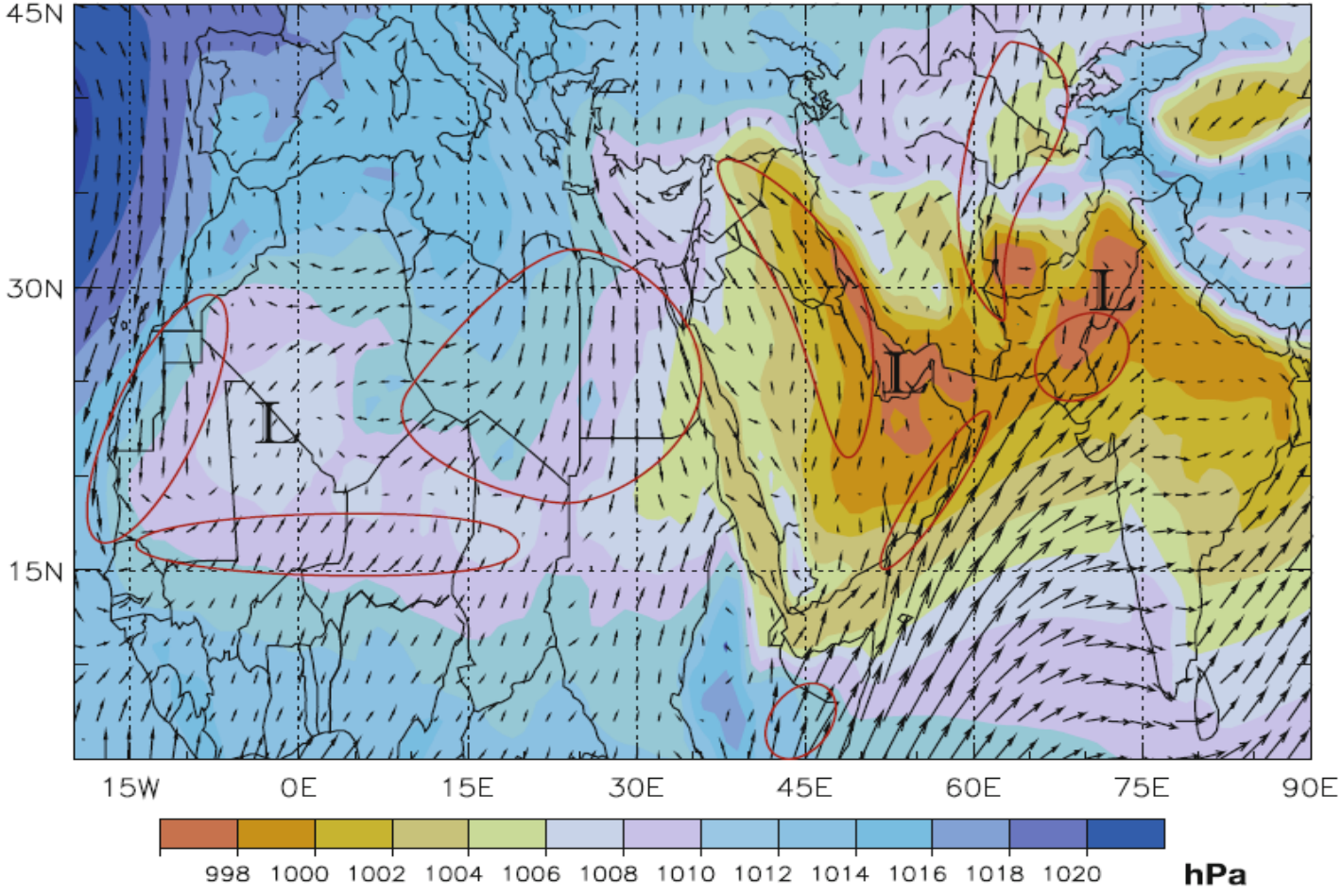

Fig. 6.1 Boreal summer (June–August) average mean sea-level pressure (*shaded*) and 10 m vector winds. The three main continental heat lows over West Africa, the Arabian Peninsula and the border of India and Pakistan are marked with 'L's. Areas with strong inflow into these heat lows prone to dust generation are marked in red. The plot is based on 1979–2012 ERA-Interim analyses produced by the European Centre for Medium-Range Weather Forecasts (ECMWF)

Synoptic scale dust transport

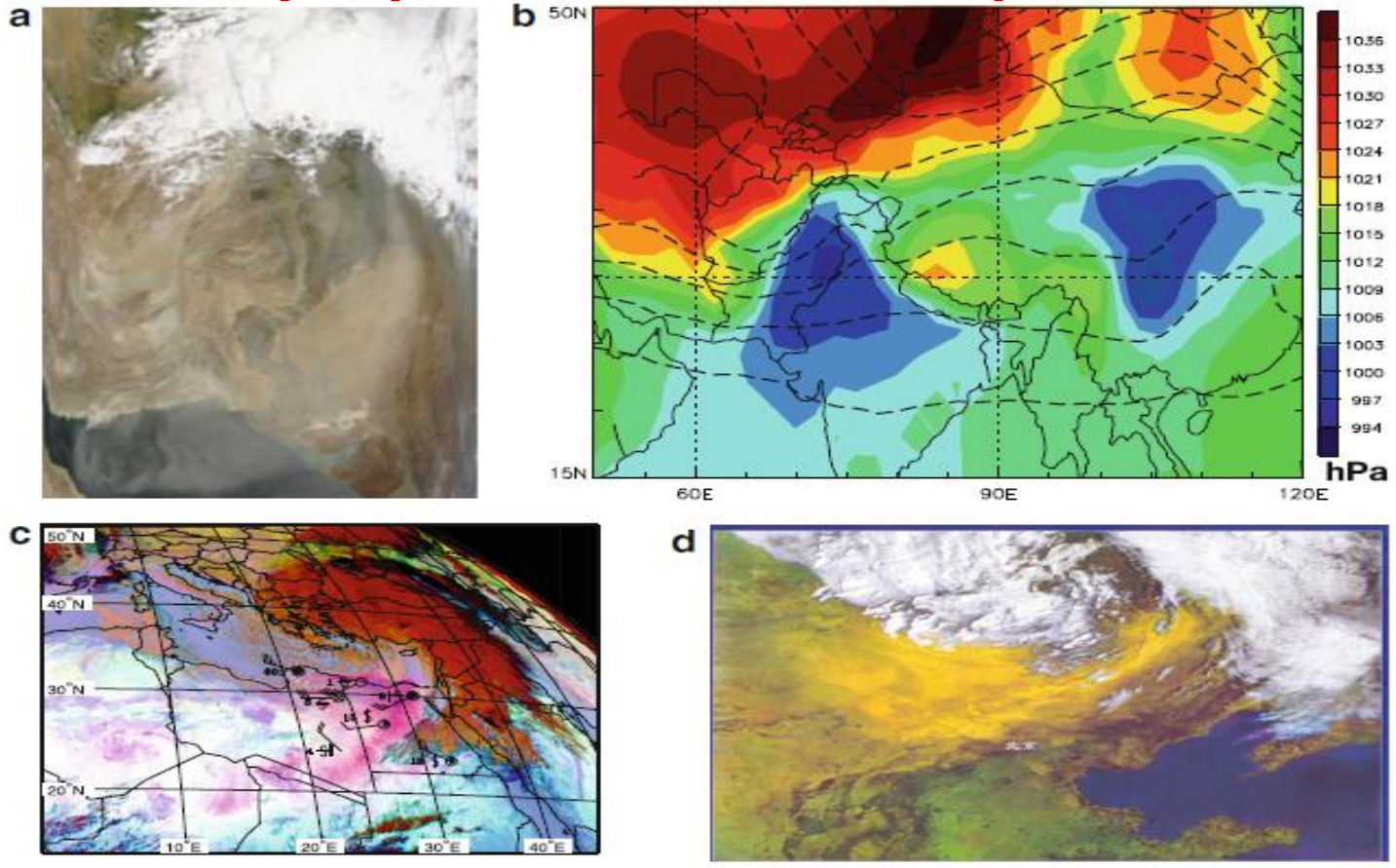

Fig. 6.3 Examples of synoptic dust storm Types I (*top*) and II (*bottom*). (**a**) MODIS Terra visible image at 0610 UTC 7 April 2005 showing an intense dust storm over India and Pakistan. (**b**) Associated patterns (at 00 UTC 7 April) of mean sea-level pressure (*shading*) and geopotential height at 500 hPa (contoured every 60 gpm) from ECMWF data. (**c**) Meteosat dust product showing a Khamsin cyclone on 22 January 2004 including some synoptic station reports indicating dust storms and strong winds (Fig. 9b in Knippertz and Todd 2012). The *dark red colours* show the main cloud mass of the cyclone and cold front, while *pink colours* indicate dust emission. (**d**) Dust storm over China as seen by the Chinese Geostationary Satellite FY-1C in the morning of 6 April 2000 (Fig. 12 in Shao et al. 2002)

Dust Devils

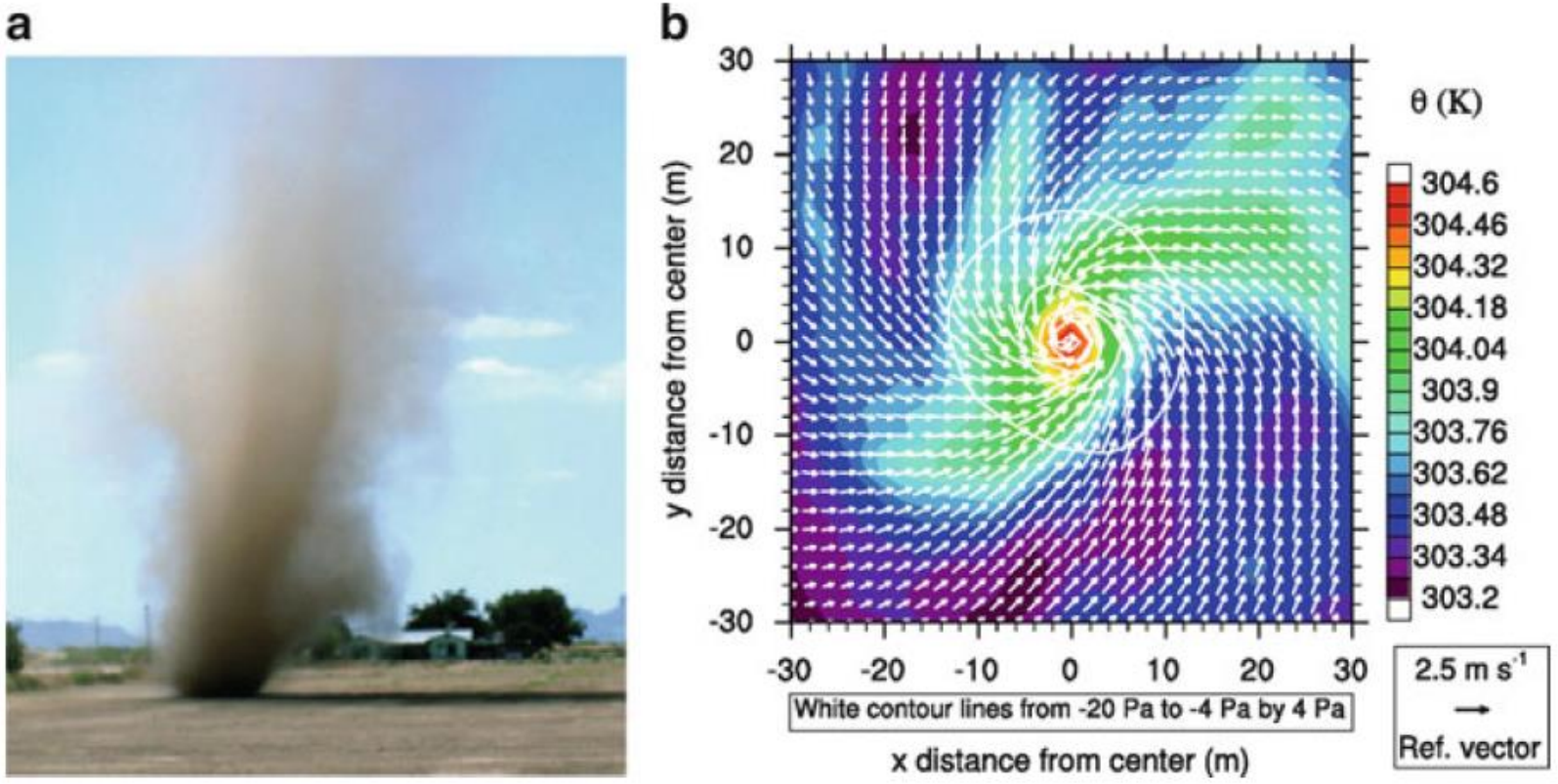

Fig. 6.8 (**a**) Photograph of a dust devil in Eloy, Arizona (Fig. 1c from Balme and Greeley 2006). (**b**) Horizontal distribution of potential temperature (*shading*), perturbation pressure (*contours*) and the horizontal component of wind vectors (*arrows*) at 1 m above ground using 2 m grid spacing (Fig. 8a from Raasch and Franke 2011)

Low Level Jets (LLJ)

03-09 UTC

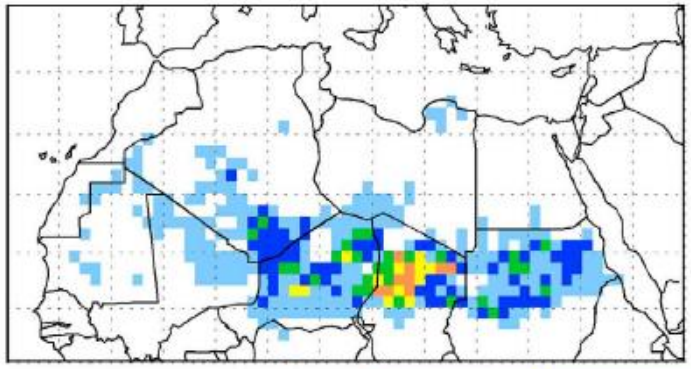

12-00 UTC

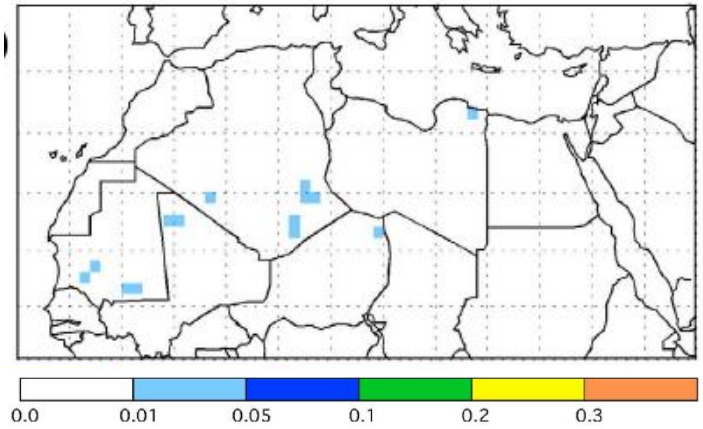

Frequency of dust source activation from the two SEVIRI infrared channels

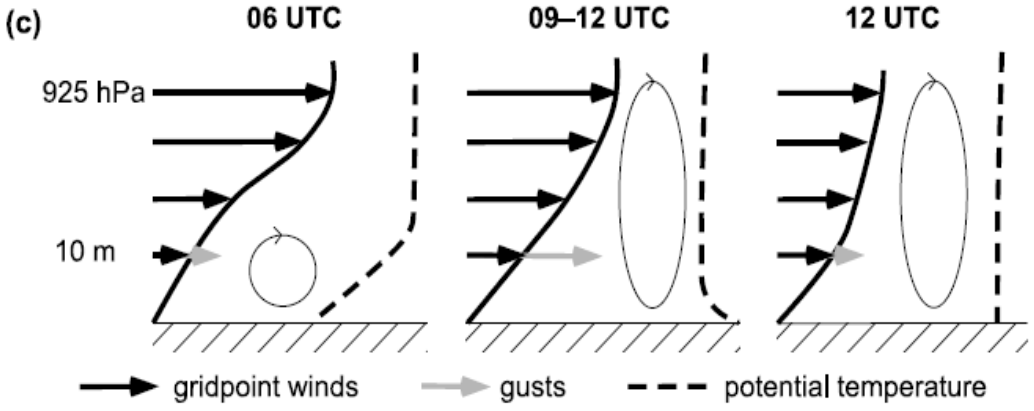

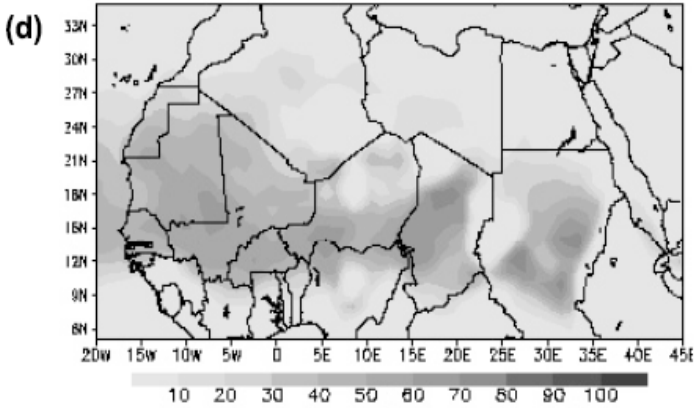

Downward mixing of momentum from the nocturnal LLJ during the morning buildup of the PBL.

Schepanski et al., JGR, 2009

Knippertz, P., and M. C. Todd, Rev. Geophys., 2012

Table 7.1 Acronyms and abbreviations of satellites, sensors, products, networks and field campaigns

AD-Net	Asian Dust Network
AERONET	Aerosol Robotic Network
AI (from TOMS and OMI)	Aerosol index
AIRS	Atmospheric Infrared Sounder
AMMA	African Monsoon Multidisciplinary Analysis
AOD	Aerosol optical depth
AVHRR	Advanced Very High Resolution Radiometer
CALIOP	Cloud-Aerosol Lidar with Orthogonal Polarization
CALIPSO	Cloud-Aerosol Lidar and Infrared Pathfinder Satellite Observation
DOD or dust AOD	Dust optical depth
EARLINET	European Aerosol Research Lidar Network
GOES	Geostationary Operational Environmental Satellite
IASI	Infrared Atmospheric Sounding Interferometer
IDDI	Infrared difference dust index
IR	Infrared
Meteosat	European Geostationary Meteorological Satellites
Metop	Meteorological operational satellite programme
MISR	Multiangle Imaging Spectroradiometer
MODIS	Moderate-Resolution Imaging Spectroradiometer
MSG	Meteosat Second Generation
MVIRI	Meteosat Visible and Infrared Imager
NOAA	National Oceanic and Atmospheric Administration
OMI	Ozone Monitoring Instrument
PARASOL	Polarization and Anisotropy of Reflectances for Atmospheric Science Coupled with Observations from a Lidar
PM2.5, PM10	Mass concentrations of particulate matter with an aerodynamic diameter smaller than 2.5, 10 μm
POLDER	Polarization and Directionality of the Earth's Reflectances
PRIDE	Puerto Rico Dust Experiment
SAMUM	Saharan Mineral Dust Experiment
SeaWiFS	Sea-Viewing Wide Field of View Sensor
SEVIRI	Spinning Enhanced Visible and Infrared Imager
SHADE	Saharan Dust Experiment
TEOM	Tapered element oscillating microbalance
TOMS	Total ozone mapping spectrometer
UV	Ultraviolet

Satellite uncertainties

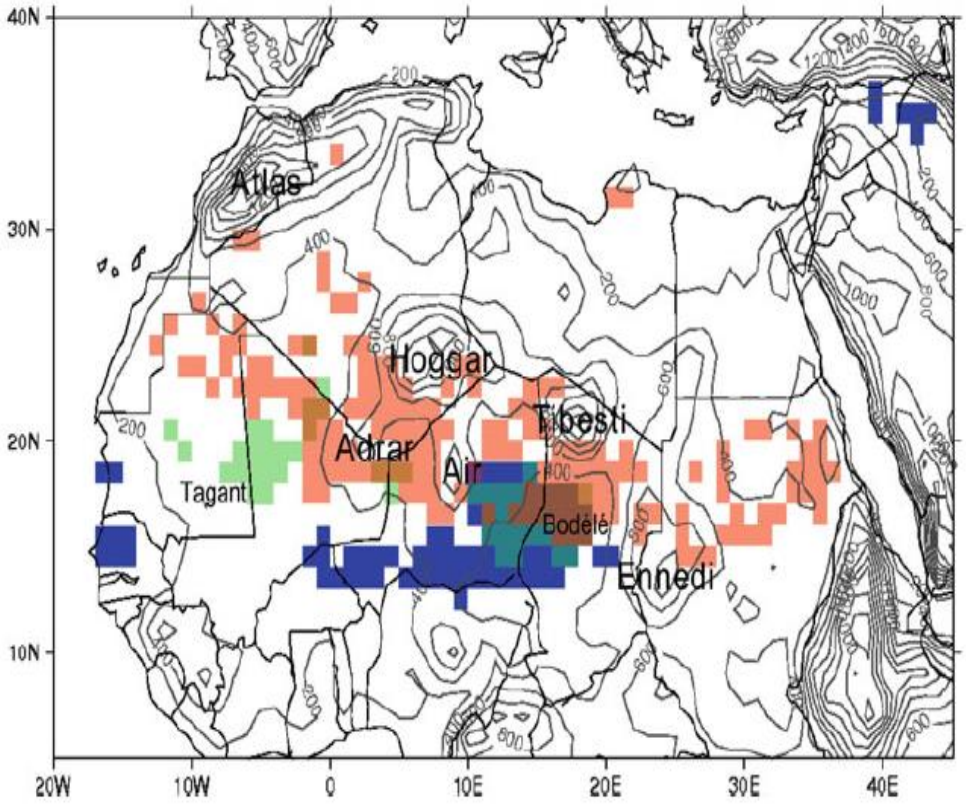

Fig. 7.3 Summary of main dust source areas inferred from satellite observations. Different colours indicate the three satellite dust products: *blue* MODIS Deep Blue AOD frequency >40 %, *green* OMI AI frequency >40 % and *red* MSG dust source activation frequency >6 %. *Contour lines* represent topography and are given at 200 m intervals. The figure illustrates the differences between the three satellite datasets in terms of identification of dust source regions (except for the Bodélé Depression) (From Schepanski et al. 2012)

- The interpretation of individual satellite dust products may be complicated by a number of factors.
- The difficulties of interpreting coarse-resolution satellite data and of differentiating between transported and emitted dust are some of them.
- In certain cases, the restriction to clear sky conditions and the contribution of aerosol species other than dust to the satellite retrieval can be problematic.
- Observations from space remain one of the most powerful tools to locate and study dust sources, particular in combination with numerical models

Why we care about atmospheric aerosols ?

1. **Aerosol related atmospheric hazards** (dust storms, volcanic ash, aerosol invigorated floods and cyclones, human health implications, visibility issues, aviation safety, etc.)
2. **Important scientific questions** regarding the role of aerosols as weather and climate regulators.

Dust cycle

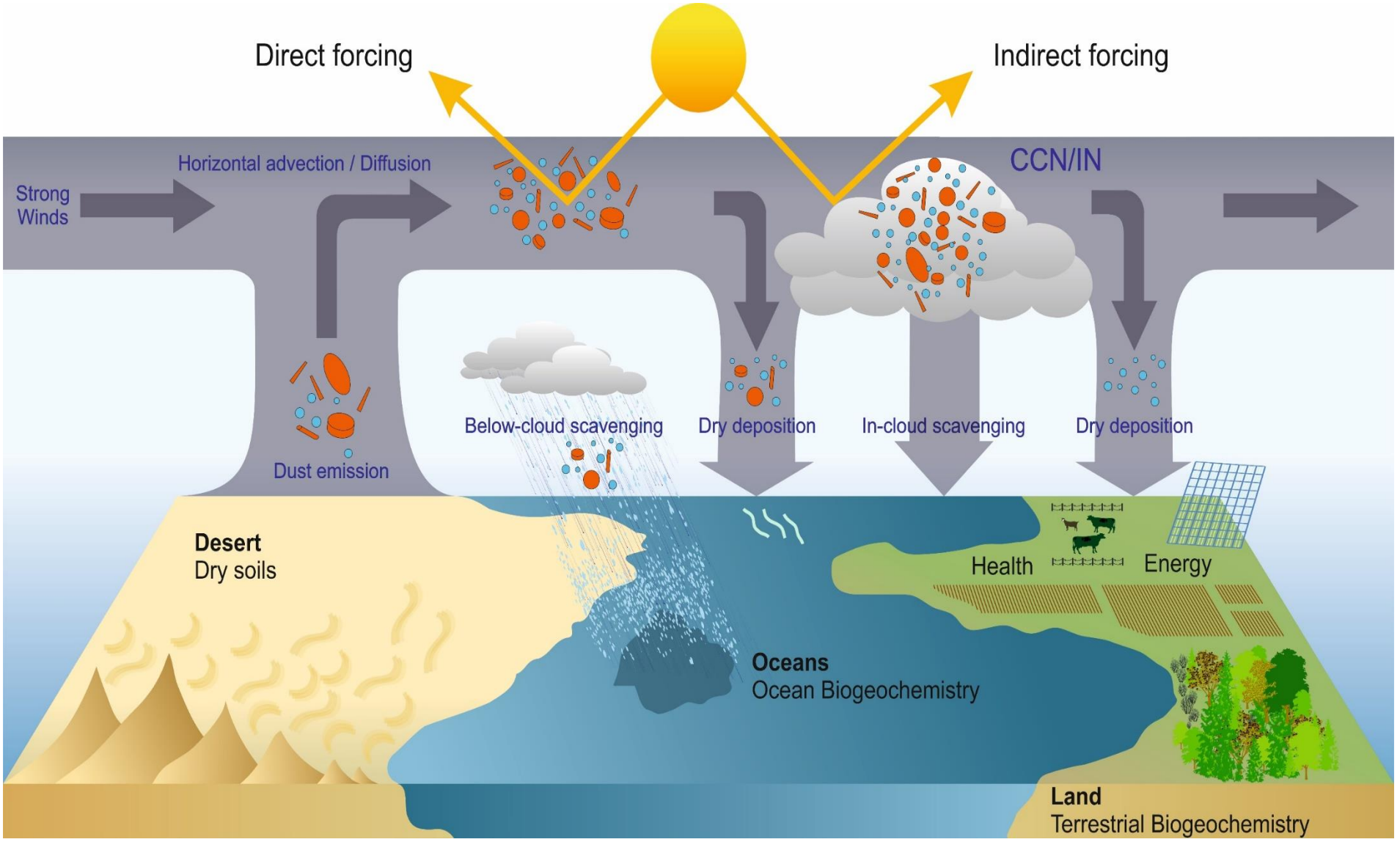
Direct forcing
Indirect forcing
Horizontal advection / Diffusion
Strong Winds
CCN/IN
Dust emission
Below-cloud scavenging
Dry deposition
In-cloud scavenging
Dry deposition
Desert
Dry soils
Health
Energy
Oceans
Ocean Biogeochemistry
Land
Terrestrial Biogeochemistry

Environmental effects of dust

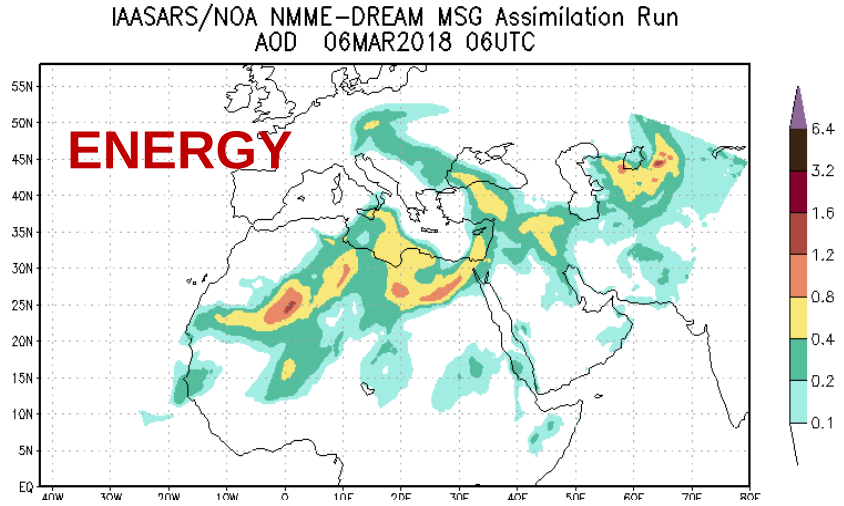

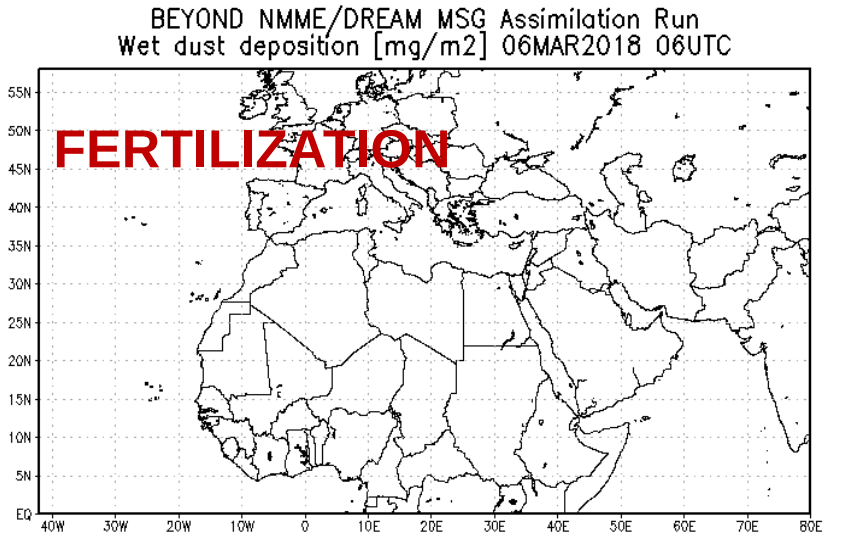

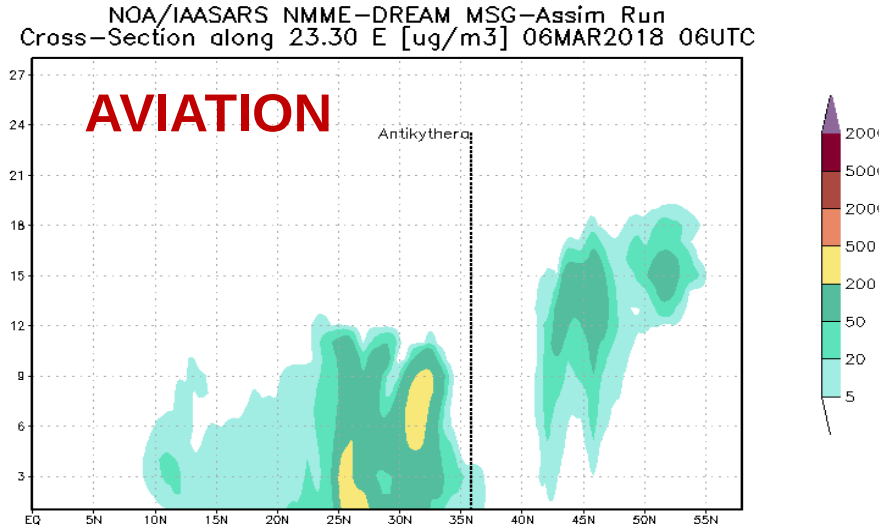

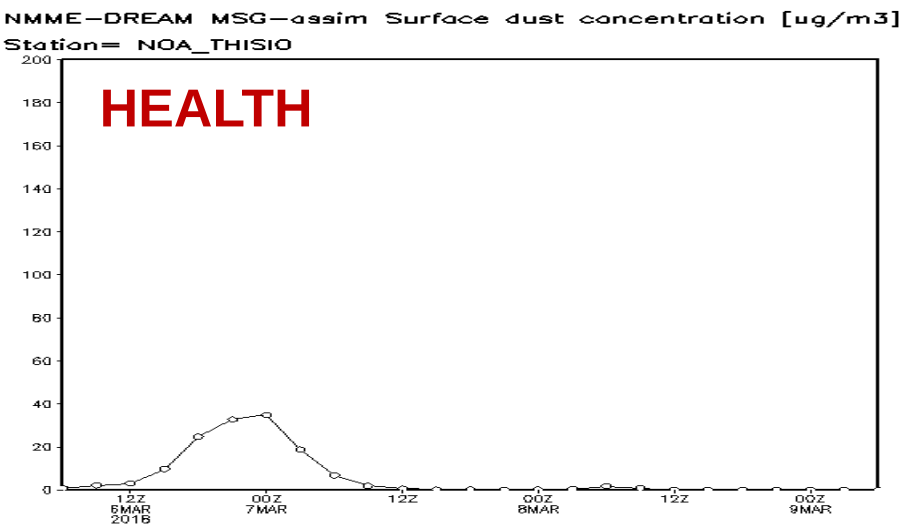

Aerosol – Atmosphere interactions

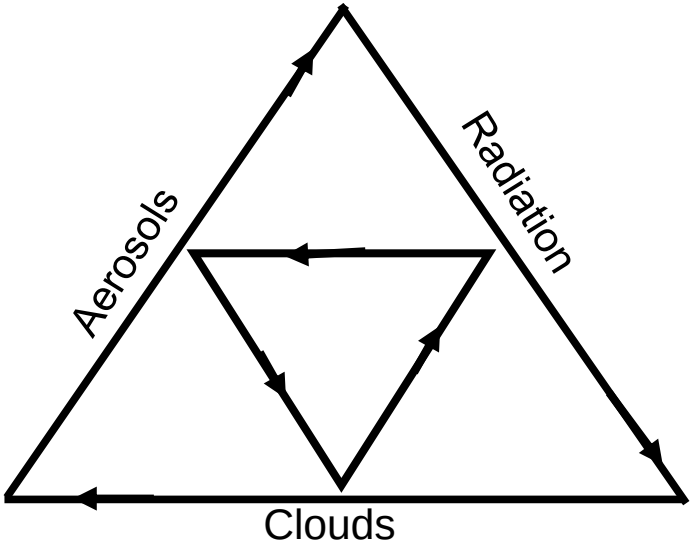

Non linear

Climate impacts

Direct Effects :

Scattering and absorption of solar and terrestrial radiation.

Indirect Effects :

"Polluted" clouds contain more cloud droplets that are smaller in size.

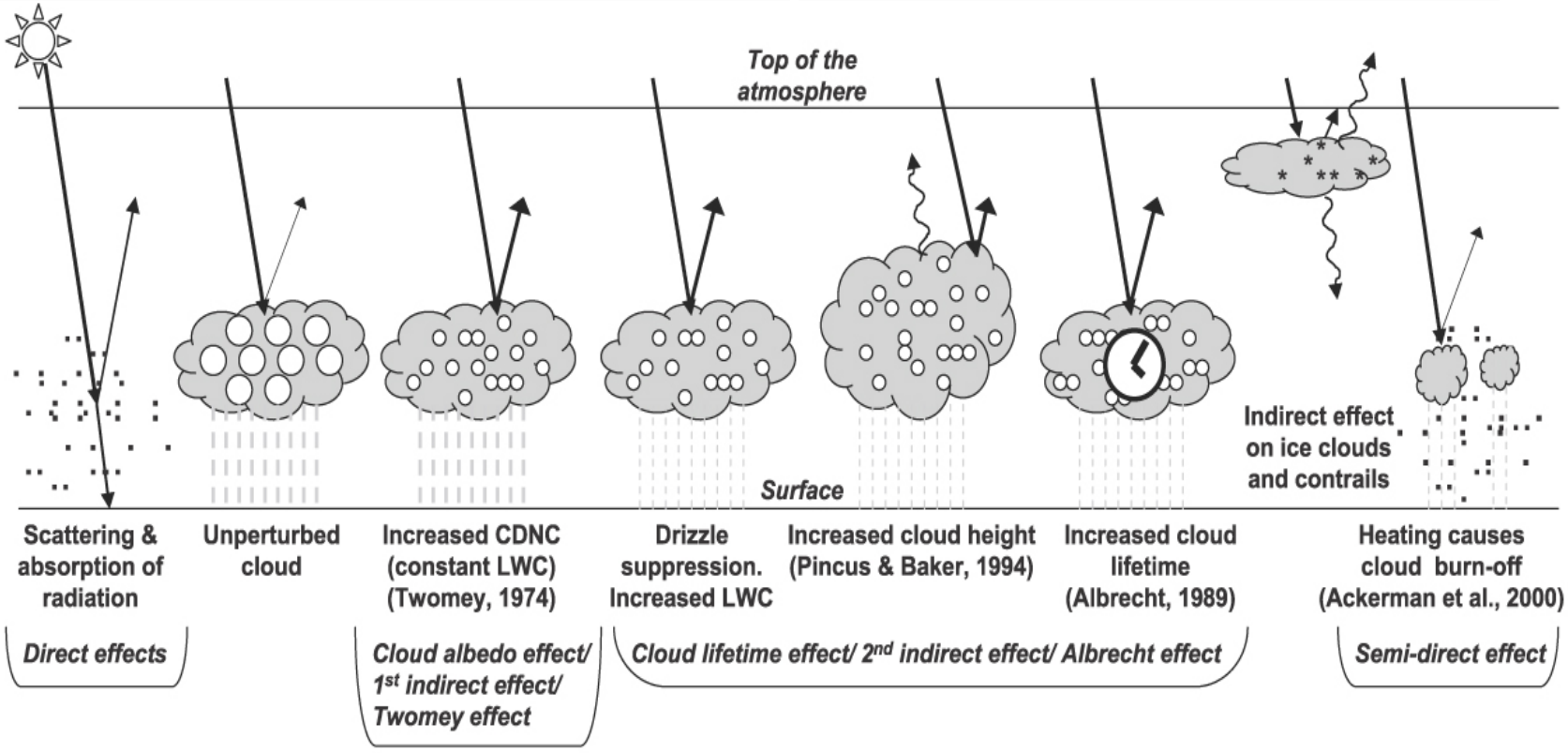

IPCC, 2007

Aerosols and Clouds (indirect effect)

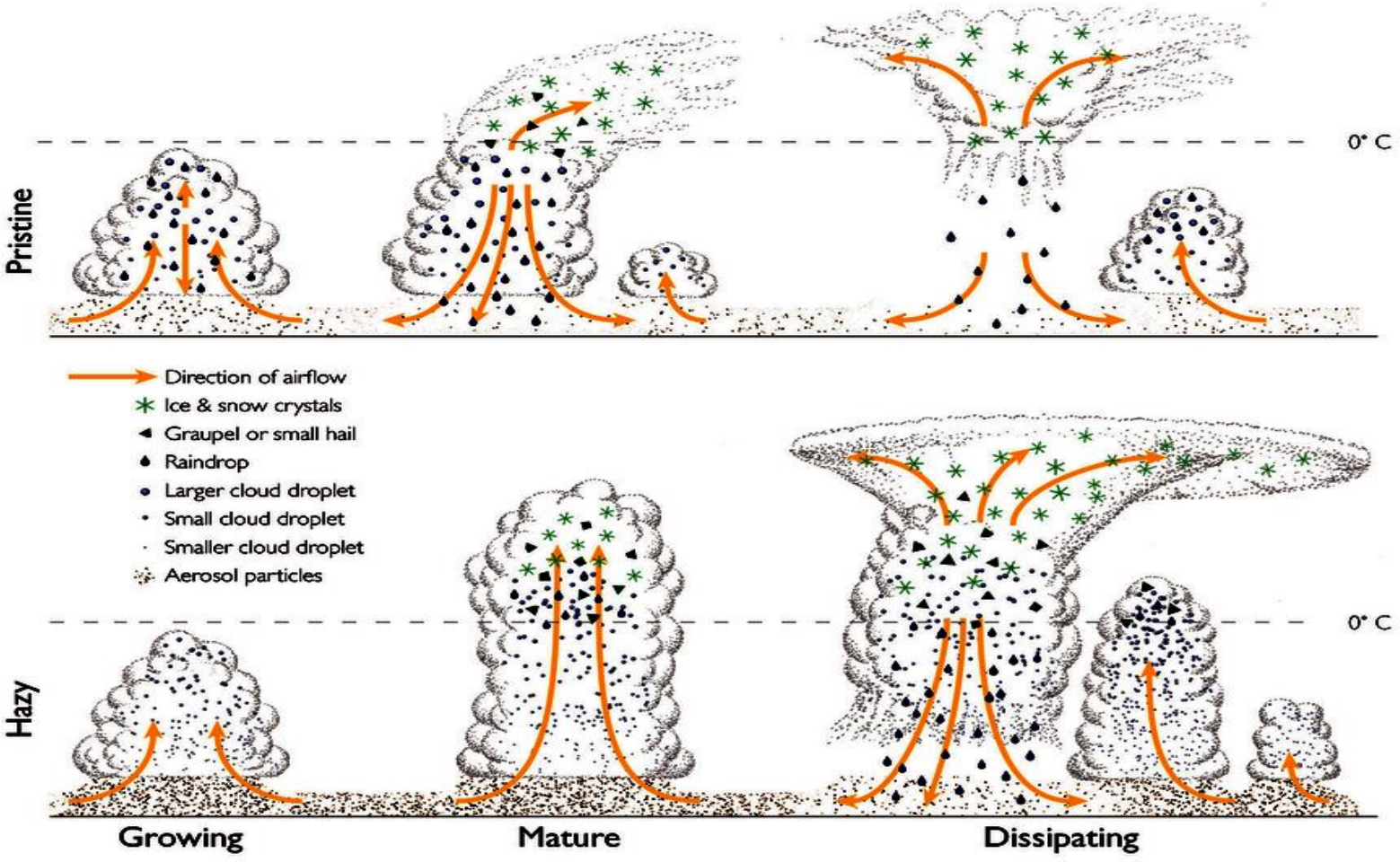

(Rosenfeld at al., Science, 2008)

Cloud Microphysics

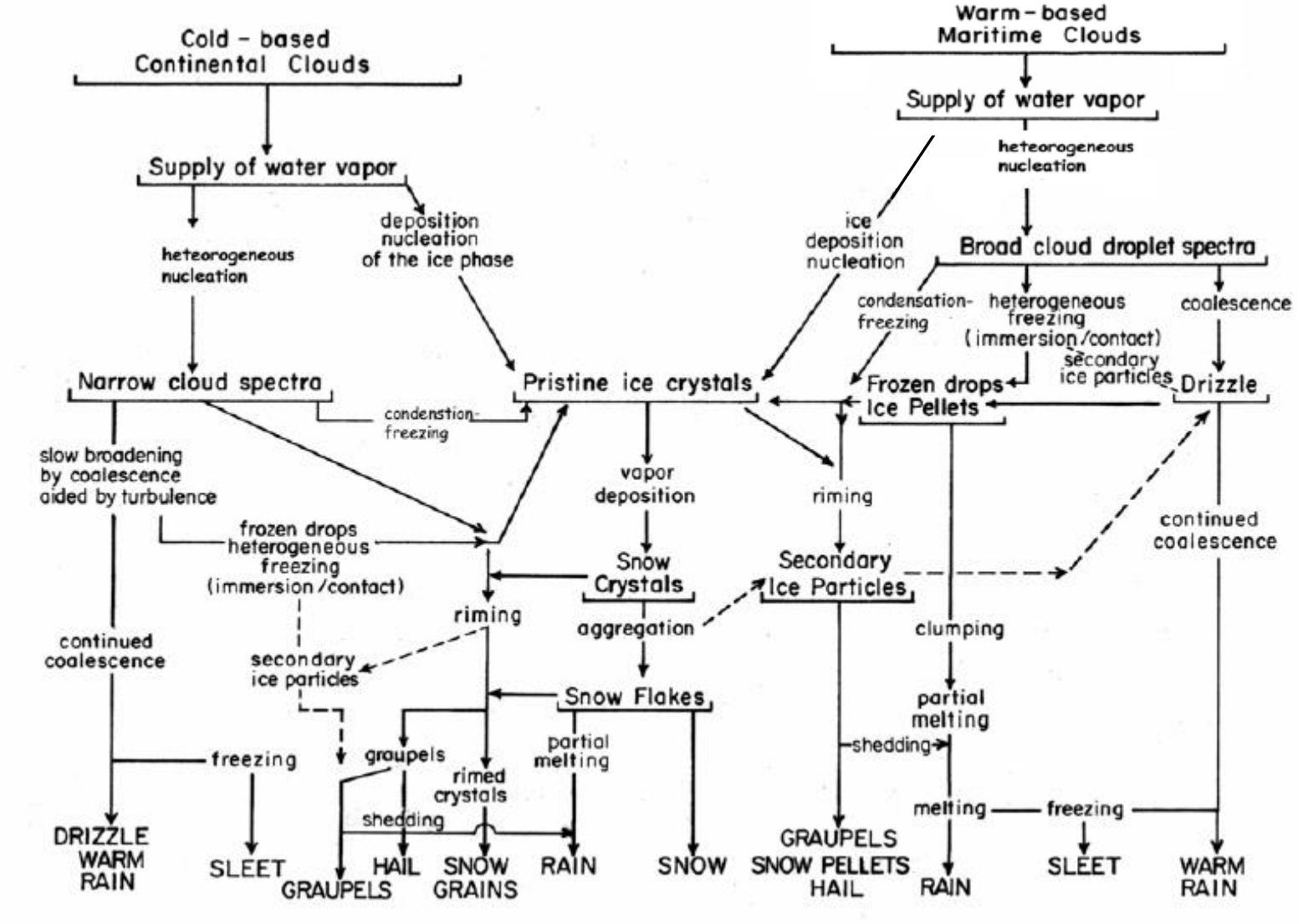

(Braham, 1968)

Dust impact on surface solar irradiance

NCEP FNL wind speed at 1000 hPa, 1200 UTC 31 January 2015

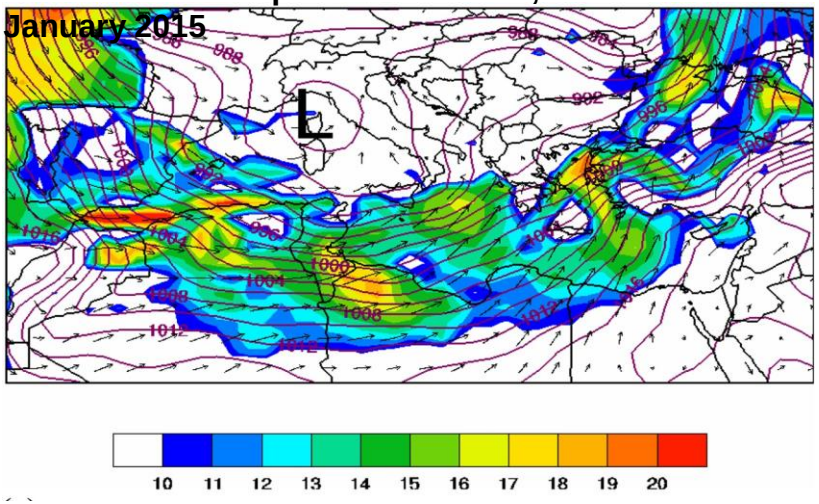

HYSPLIT backtrajectories, 1200 UTC 1

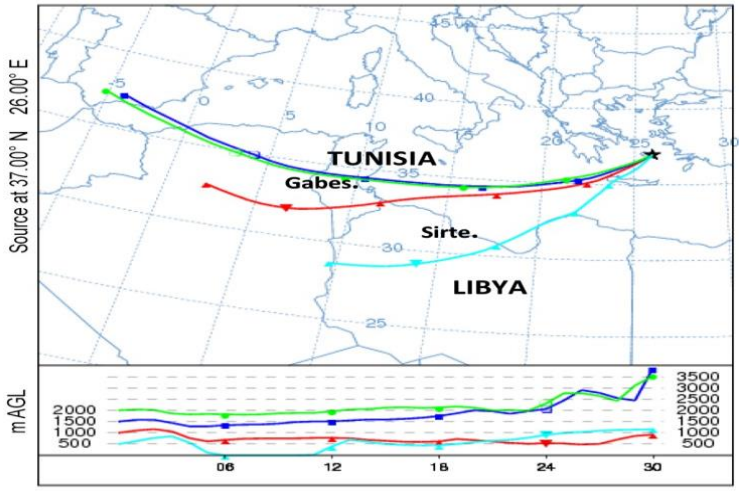

MODIS & CALIPSO overpass, 1 February 2015

Kosmopoulos et al., 2017, AMT

MYD04 L2 006 optical depth land and ocean 550 nm 2015-02-01

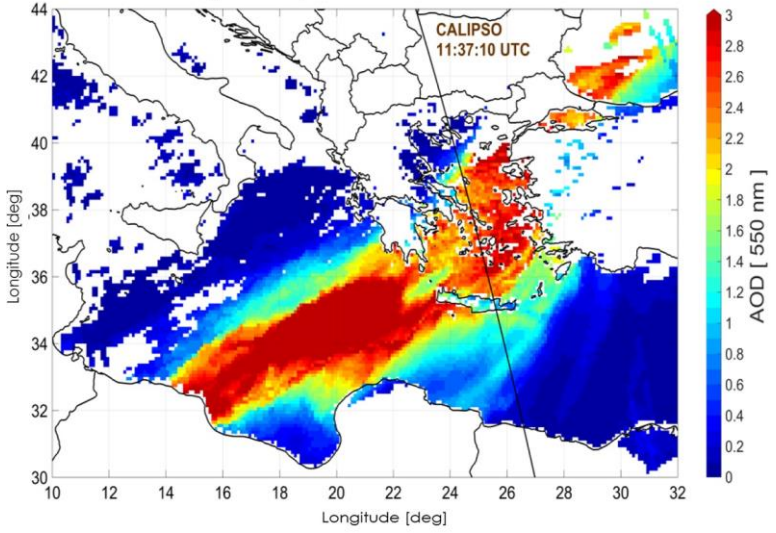

CALIPSO aerosol extinction coefficient at 532 nm
2015-02-01, 11:37:10 UTC

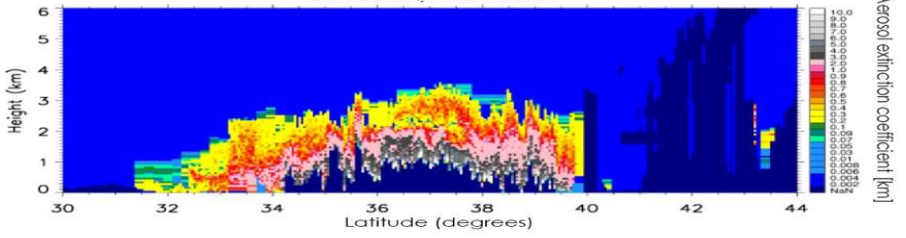

CALIPSO aerosol subtype, 2015-02-01, 11:37:10 UTC

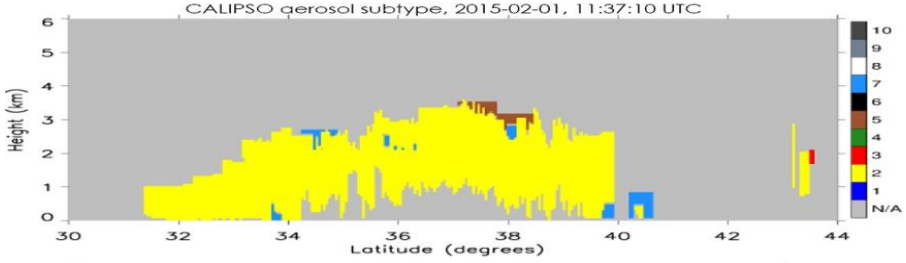

N/A: not applicable 1: Marine 2: Dust 3: Polluted continental/smoke
4: Clean continental 5: Polluted dust 6: Elevated smoke 7: Dusty marine
8: PSC aerosol 9: Volcanic ash 10: Sulfate/other

Dust impact on surface solar irradiance

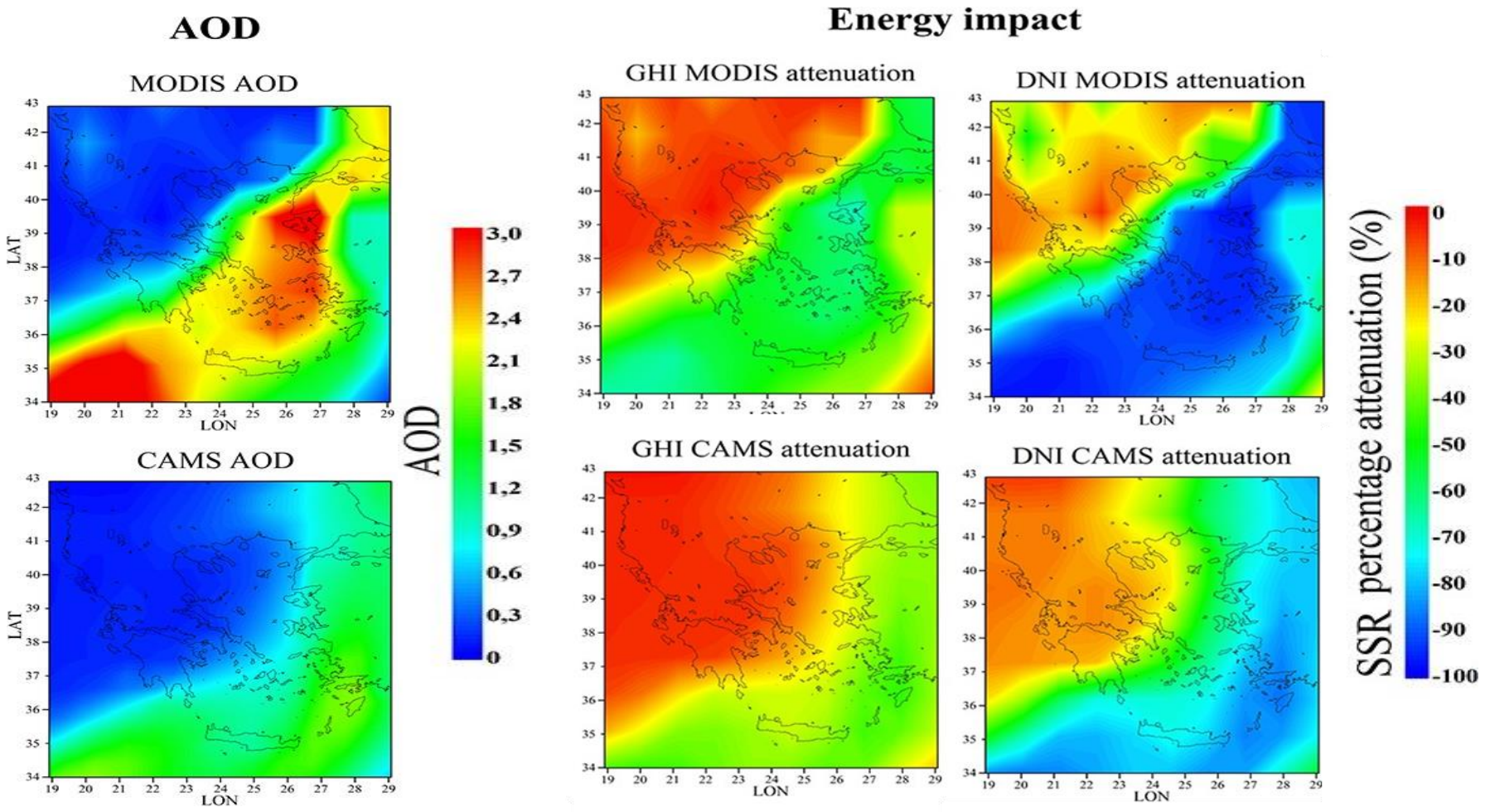

Photovoltaic (**PV**) exploit the Global Horizontal Irradiance (**GHI**)

libRadtran Radiative transfer model

Concentrated Solar Power (**CSP**) exploit the Direct Normal Irradiance (**DNI**)

Aerosol Monitoring - Observational Platforms

Our Lab is the sky

Ground- based

- In situ
- Columnar
- Profiling

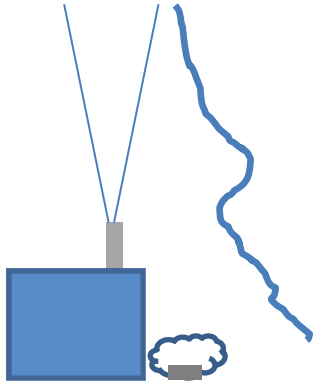

Air-borne

- In situ
- Columnar
- Profiling

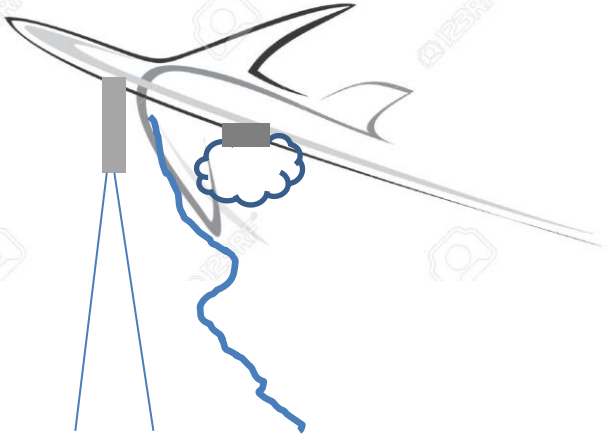

Satellite-borne

- Columnar
- Profiling

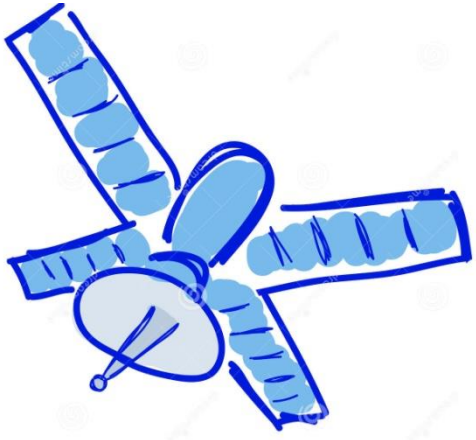

- Different coverage in time and space
- Differences in representativeness of the measurements

Aerosol Monitoring - Remote Sensing Platforms

Photometers

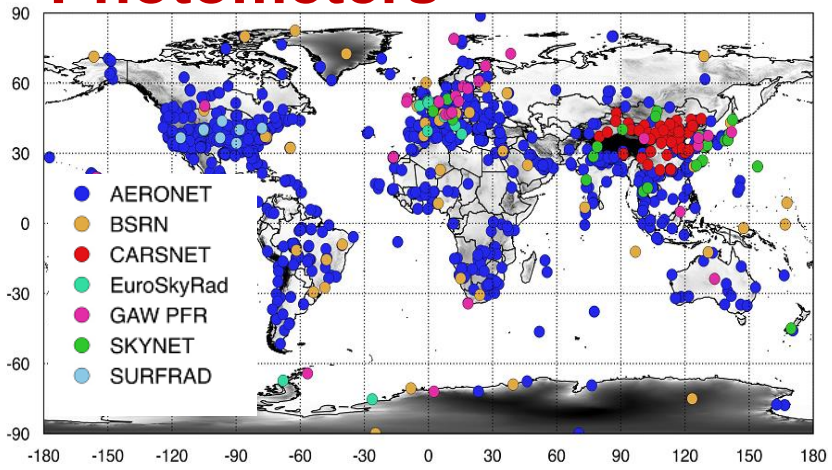

Lidars

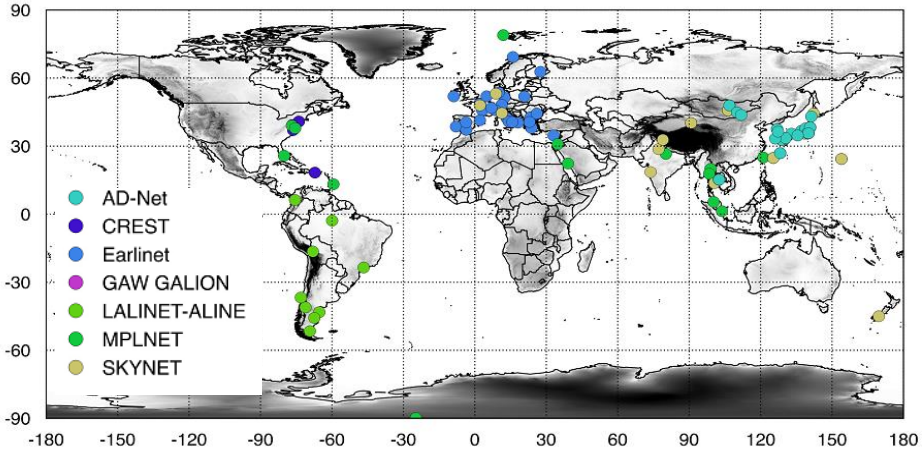

Ceilometers

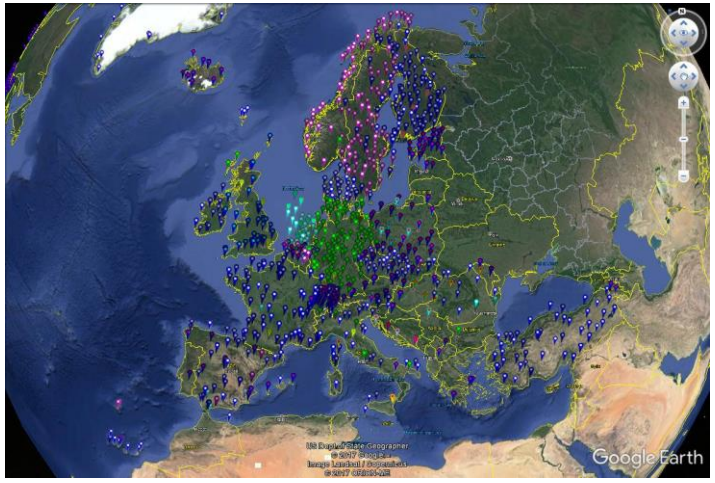

Satellite

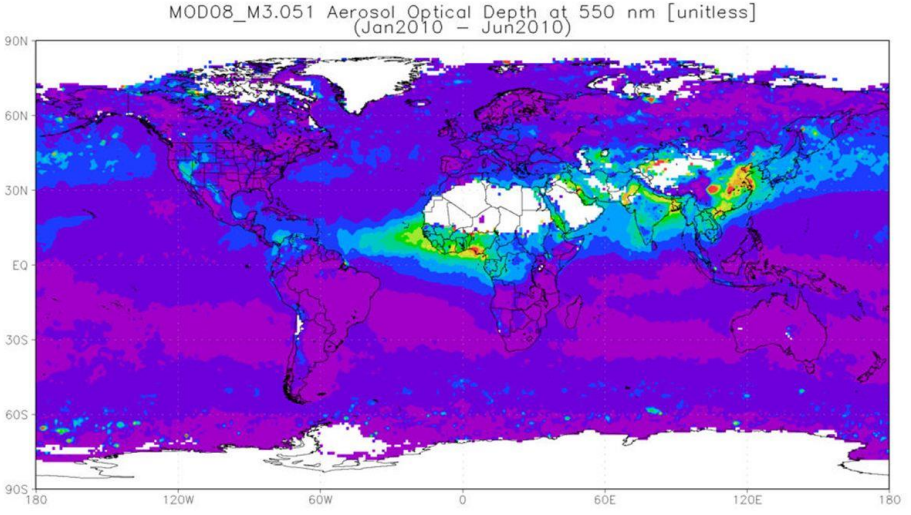

Photometers

Network	Abbreviations	Main instrument	Region	Website
AERONET	Aerosol Robotic network	Sun – sky – lunar photometer	Global	https://aeronet.gsfc.nasa.gov/
BSRN	Baseline surface radiation network	Radiometer, Pyrheliometer, Pyranometer, Pyrgeometer	Global	http://bsrn.awi.de/
CARSNET	China Aerosol Remote Sensing Network	Sun photometers	China / Asia	--
EuroSkyRad	European Skynet Radiometers network	Sky-sun photometer	Europe / USA	http://www.euroskyrad.net/
GAW PFR	Global Atmosphere Watch – Precision filter radiometer network	Precision filter radiometer	Global	http://www.pmodwrc.ch/worcc/
SKYNET	(Sky radiometers network)	Sky radiometer	Asia / Europe	http://atmos2.cr.chiba-u.jp/skynet/
SURFRAD	Surface radiation network	MRS radiometer	USA	https://www.esrl.noaa.gov/gmd/grad/surfrad/

Lidars & ceilometers

Network	Abbreviation	Region	Website
AD-NET	Asian-Dust and Aerosol Ldar Network	Japan / Asia	http://www-lidar.nies.go.jp/AD-Net/
LALINET	Latin American Lidar Network	South America	http://www.lalinet.org/
CIS-LiNet	CIS Lidar Network	Europe / Asia	--
EARLINET	European Aerosol Research Network	Europe	https://earlinet.org
MPLNET	Micro-Pulse Lidar Network	Global	https://mplnet.gsfc.nasa.gov/
NDACC	Network for the Detection of Atmospheric Composition Change	Global	http://www.ndsc.ncep.noaa.gov/
CREST	Cooperative Remote Sensing Science and Technology	USA	http://noaacrest.umbc.edu/crest-lidar-network/
E-PROFILE	Part of EUMETNET ‘s EUCOS	Europe	http://eumetnet.eu/activities/observations-programme/current-activities/e-profile/
NMHS Ceilometers	National meteorolgical and hydrological services ceilometers	Global	--
SKYNET (maxdoas)	(Sky radiometers network)	Japan	http://atmos2.cr.chiba-u.jp/skynet/

Non resolved dust sources

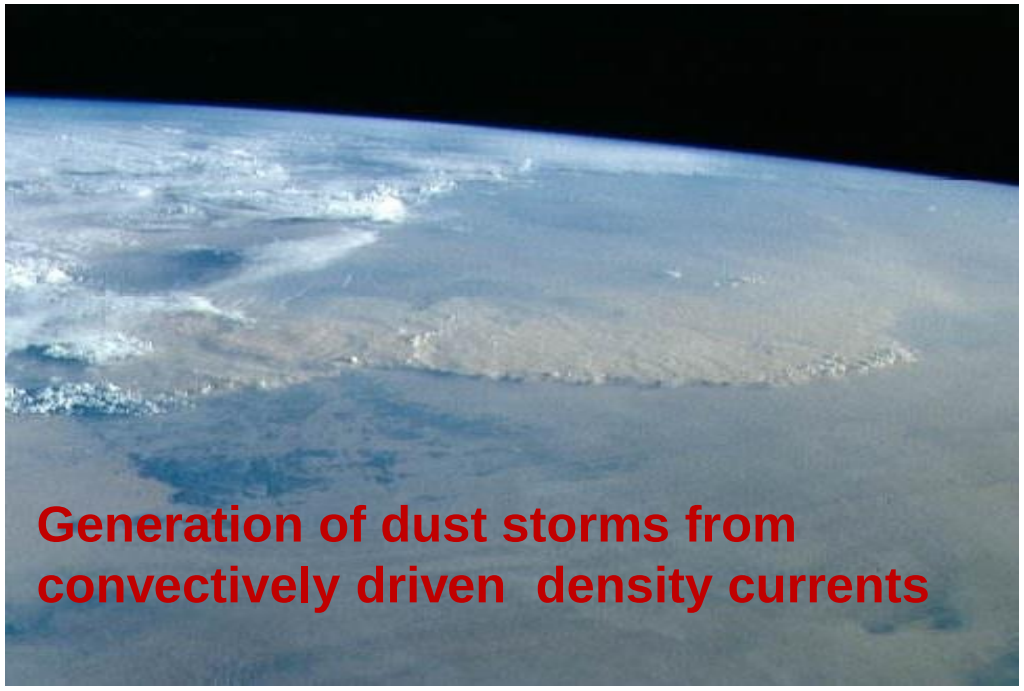

Dust Mineralogy
Dust particles from different sources have different chemical and optical properties (e.g. lidar ratio) and follow different size-distributions.

Desertification and seasonal dust emissions from drained lakes (e.g. Aral lake)

Dust experimental campaigns

Scientific problems being addressed

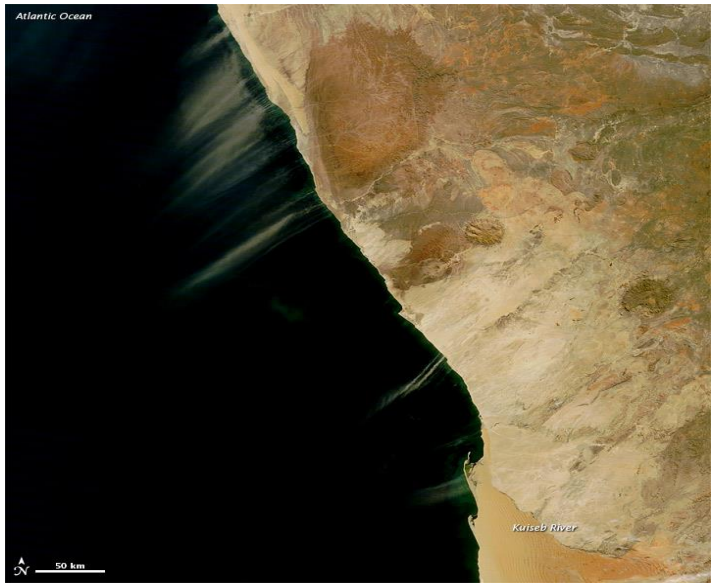

Satellite images of dust plumes blowing from the coastal arid areas (top) and from the dry lake Etosha Pan (down)

- Namibian dust has not been yet widely examined neither by in-situ experiments nor by remote sensing or modeling studies.
- The collocation of airborne dust originating from sources with different mineralogy provides an ideal opportunity to apply remote sensing methodologies for the characterization of these particles and examine their optical and microphysical properties.
- Improve the description of modeled dust in the area by assimilating satellite dust retrievals (MSG-SEVIRI, CALIPSO and CATS) in a regional atmospheric model (NMM-DREAM).

ASKOS campaign at Cape Verde 2020

Lidar

Atmospheric Modeling

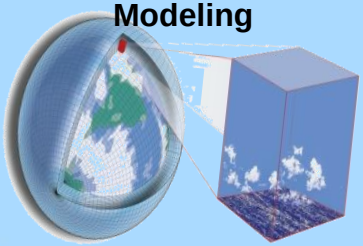

Cloud radar

Airborne remote sensing & in situ

Barbados — **Cape Verde**

0 — 1.000,00 χιλιόμετρα — 3.000,00 χιλιόμετρα

Cloud Condensates

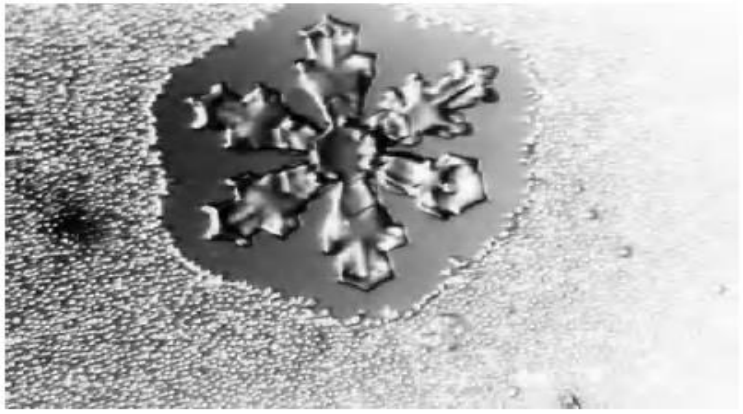

Fig. 6.36 Laboratory demonstration of the growth of an ice crystal at the expense of surrounding supercooled water drops. [Photograph courtesy of Richard L. Pitter.]

Fig. 6.37 The growing cumulus clouds in the foreground with well-defined boundaries contained primarily small droplets. The higher cloud behind with fuzzy boundaries is an older glaciated cloud full of ice crystals. [Photograph courtesy of Art Rangno.]

Fig. 6.38 Fallstreaks of ice crystals from cirrus cloud characteristic curved shape of fallstreaks indicates th wind speed was increasing (from left to right) with incr altitude. [Photograph courtesy of Art Rangno.]

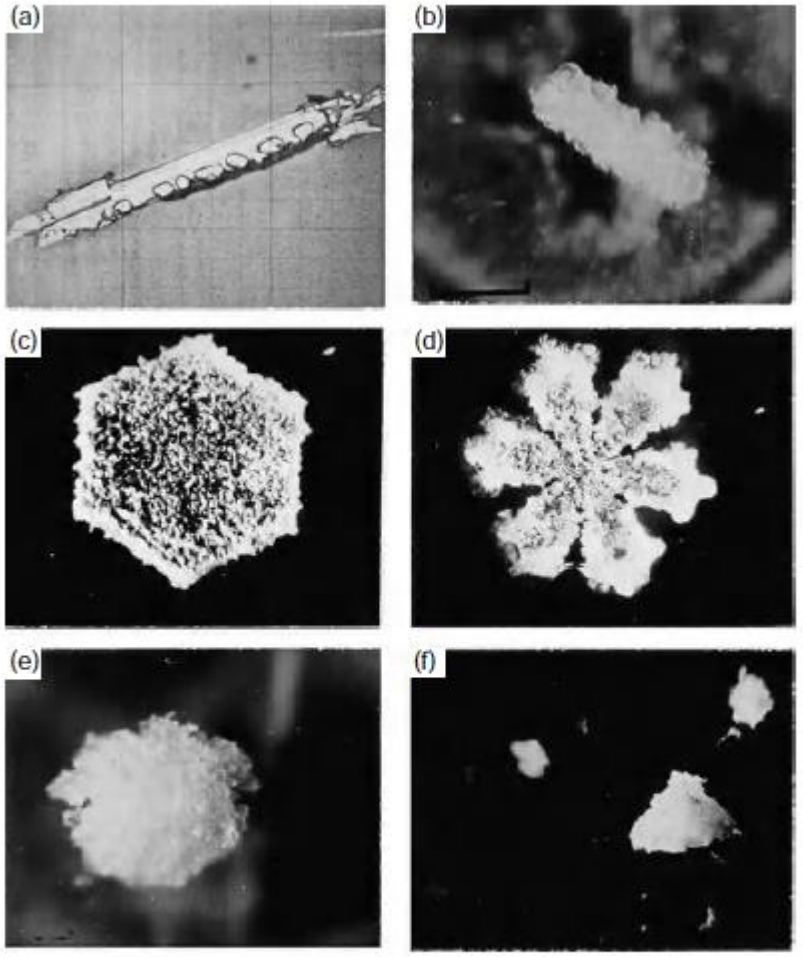

Fig. 6.41 (a) Lightly rimed needle; (b) rimed column; (c) rimed plate; (d) rimed stellar; (e) spherical graupel; and (f) conical graupel. [Photographs courtesy of Cloud and Aerosol Research Group, University of Washington.]

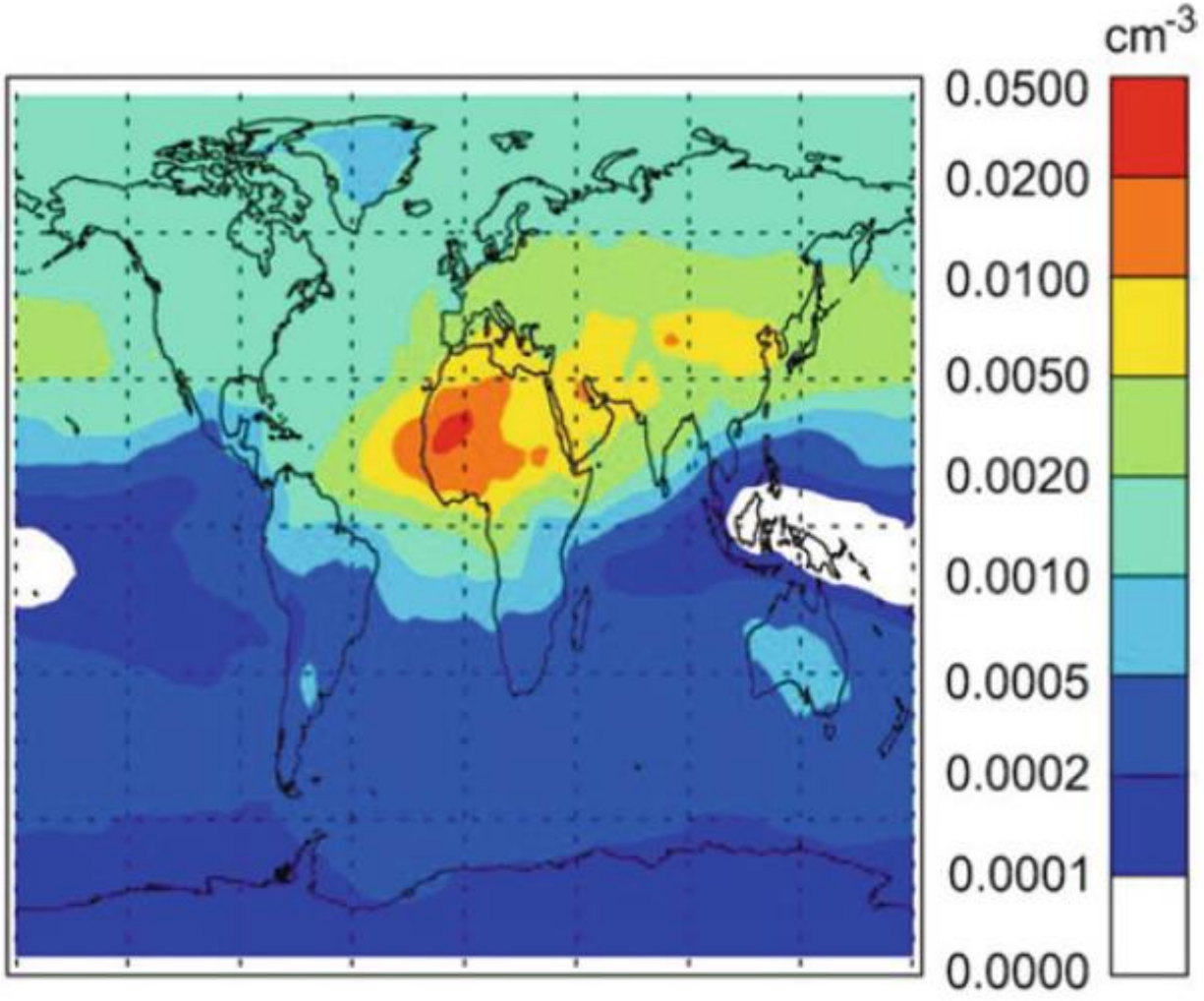

Fig. 12.9 Annual average mineral dust IN concentrations at 600 hPa active at −20 °C. The IN concentration is based on the modeled K-feldspar content of airborne mineral dust (This figure is reproduced from Atkinson et al. (2013))

NOA Climate Change Observatory in Antikithira